A synergistic damage mechanics approach to mechanical response of composite laminates with ply cracks

Chandra Veer Singh[1] and Ramesh Talreja[2,3]

Abstract

We treat selected test cases in the third world wide failure exercise by the approach described as synergistic damage mechanics. This approach utilizes micromechanics and continuum damage mechanics to predict the overall mechanical response of composite laminates with ply cracking in multiple orientations. The material constants needed in the continuum damage mechanic formulation are calculated from stiffness property changes incurred in a reference laminate. For other laminate configurations, the stiffness changes are derived using a relative constraint parameter which is calculated from the constraint on the opening displacement of ply cracks within the given cracked laminate evaluated numerically by a finite element analysis of appropriately constructed representative unit cell. The number density of ply cracks (cracks per unit length normal to the crack planes) under quasi-static loading is calculated by an energy-based approach. Finally, the stress–strain response of a laminate is determined by combining stiffness property changes and evolution of crack number density.

Introduction and historical background

Failure analysis of composite materials is currently performed by the industry using empirical criteria, none of which properly accounts for the effects of damage processes prior to complete failure. Significant developments in the past three decades suggest that accounting for sub-critical damage will improve composite design. While previous exercises[1,2] focused on the ultimate failure, the third world wide failure exercise (WWFE-III)[3] provides an opportunity to examine initiation and progression of sub-critical events and their effect on the mechanical response.

In composite laminates, which are the subject of examination in WWFE-III, the damage initiation processes begin at the constituent level within a ply. In most cases, ply cracks span the thickness and width of the ply at relatively low loads. Subsequent loading then results in multiplication of these cracks. It is common, therefore, to start the analysis with assumed presence of ply cracks and examine their evolution (increase in number per unit length normal to crack planes) as well as the effect of these cracks in changing the laminate-averaged mechanical properties. The

approaches taken to address this problem can be broadly characterized as micro-damage mechanics (or simply, micromechanics), e.g. shear-lag methods, see for example References [4–6], and continuum damage mechanics (CDMs). Our current approach is to retain the framework of CDM but enrich its capabilities by combining it with micromechanics. We have called this approach synergistic damage mechanics (SDM). The present paper will first briefly describe the SDM methodology and then apply it to selected cases of WWFE-III.

The CDM[7,8] uses a physically based damage characterization that does not leave behind essential features of damage in the context of the material response of

[1]Department of Materials Science and Engineering, University of Toronto, Toronto, ON, Canada
[2]Department of Aerospace Engineering, Texas A&M University, College Station, TX, USA
[3]Visiting Professor, Luleå University of Technology, Luleå, Sweden

Corresponding author:
Ramesh Talreja, Department of Aerospace Engineering, Texas A&M University, College Station, TX 77843-3141, USA.
Email: talreja@aero.tamu.edu

interest while keeping in sight practical implementation of the resulting methodology. As argued in References [7,8] and elaborated further in References [9–11], a scalar-valued characterization would be inadequate in view of the oriented nature of the internal surfaces formed. Although a vector-valued characterization was employed at first, the issue of ambiguity of the sense of a vector could be addressed more elegantly by using a second order tensor instead. The damage characterization for ply cracking involved calculation of a constraint parameter, κ, which essentially captures the environment of the cracked surfaces (e.g. effect of surrounding plies), and a number of damage constants, c_i which depend on the laminate material. These constants will be described later. The observation that the κ-parameter may be viewed as a carrier of the local effects on damage entities within a 'Representative Volume Element' (RVE), while the c_i-constants are material constants, led to a number of studies to explore prediction of elastic property changes due to damage in different modes. To be sure, the elastic properties are the averages over appropriate RVEs. CDM model considered here predicts effective stiffness changes for the whole laminate; layer-wise (or lamina-wise) CDM model have also been developed.[12,13]

At first it was found that from changes in E_x and v_{xy} due to transverse cracking in $[0/90_3]_s$ glass/epoxy laminates reported in Reference [14] and assuming no changes in E_y, changes in E_x for the same glass/epoxy of $[0/90]_s$ configuration could be predicted with good accuracy. Also, in $[0/\pm45]_s$ laminate of the same glass/epoxy, the change in E_x could be predicted by setting damage parameters $D(+45) = D(-45)$ (a good approximation, supported by crack density data). These results have been reported in Reference [9].

Later, a systematic study of the effect of constraint on the constraint parameter was done by experimentally measuring the crack opening displacement (COD) in $[\pm\theta/90_2]_s$ laminates[15–17] for different θ-values. By relating these values to the COD at $\theta = 90°$ and normalized by a unit applied strain, the predictions of E_x and v_{xy} for different θ could be made. Another study of the constraint effects was made by examining $[0/\pm\theta_4/0_{1/2}]_s$ laminates, where the ply orientation θ was varied. Once again, using experimentally measured COD for $\theta = 90°$ as the reference, the κ-parameter for other ply orientations was evaluated from the COD values and E_x and v_{xy} for different θ were predicted.[18]

While the experimental studies supported the idea of using the constraint parameter as a carrier of local constraints, the scatter in test data and the cost of testing do not make the experimental approach attractive. Therefore, another systematic study of $[0_m/\pm\theta_n/0_{m/2}]_s$ laminates was undertaken[19,20] where computational micromechanics was employed instead of physical

testing as a means of evaluating the constraint parameter. An elaborate parametric study of the constraint parameter allowed developing a master curve for elastic property predictions. The most recent study[21] examines damage modes consisting of transverse ply cracks as well as inclined cracks of different orientations in $[0_m/\pm\theta_n/90_r]_s$ and $[0_m/90_r/\pm\theta_n]_s$ laminates. The SDM approach is developed and its predictions are compared with available experimental data for $[0/90/-45/+45]_s$ laminate.

At the current state of its development, the SDM methodology has the ingredients of a multiscale damage mechanics depicted in Figure 1. As illustrated there, structural (macro-scale) analysis of a part containing damage is accomplished by a meso-scale SDM analysis of appropriate RVE in which micro-scale input from micromechanics (computed CODs) as well as materials constants from a reference laminate configuration are entered. What remains is to codify this approach in software to be used by design engineers.

Theoretical details

Definition of damage

Consider a continuum body of a composite solid with a matrix and embedded reinforcements as well as a multitude of damage entities in the form of microcracks. In CDM, the material microstructure, e.g., distributed fibres, and the distributed damage, which may be called the micro-damage structure, are treated as smeared-out fields. For evaluating the effective properties of the continuum body, the continuum is homogenized using a two-step homogenization procedure (see Figure 2). As illustrated in the figure, the material microstructure is viewed as consisting of "stationary" entities, e.g., fibres and plies, and the micro-damage structure is considered as a family of evolving entities, e.g., cracks and voids. First the stationary microstructure is smeared into a homogeneous, anisotropic material. In the next step, the evolving microstructure is replaced by a homogeneous field represented by suitable internal variables. The internal **micro-damage** structure evolves with loading and causes changes of the overall response (properties) of the composite.

Resorting to Figure 2 again, consider a generic point P inside the damaged composite body. Let an element of volume V contain a representative sample of damage entities about this point. An individual damage entity (a crack or a void) can be viewed as bounded by a surface S, on which any point can be associated with two vectors, one of which, $\boldsymbol{a}$, represents a selected influence of the damage entity, and the other, $\boldsymbol{n}$, is the unit outward normal to the surface. Let the surface integral of dyadic product of the vector components $a_i n_j$ be

COMPUTATIONAL MICROMECHANICS

Determine average COD ($\overline{\Delta u_2}$) and constraint parameters κ_θ, κ_{90} and $\kappa_{90_{2n+r}}$ from the FE model of a representative unit cell

Structural scale: Micro

EXPERIMENTAL/ COMPUTATIONAL

Evaluate damage constants a_i' using experimental or computational results for reference laminate configuration $[0_m/90_{2n+p}]_s$

SYNERGISTIC DAMAGE MECHANICS

Use SDM to determine stiffness reduction in present laminate configuration $[0_m/\pm\theta_n/90_r]_s$

Structural scale: Meso

STRUCTURAL ANALYSIS

Analyze overall structural response to external loading using the reduced stiffness properties

Structural scale: Macro

Figure 1. Multiscale synergistic methodology for analyzing damage behaviour in a general symmetric laminate $[0_m/\pm\theta_n/90_r]_s$ with matrix cracks in $+\theta$, $-\theta$ and $90°$ layers.

Stationary microstructure

Evolving microstructure

RVE for damage characterization

Step 1 Homogenization of stationary microstructure

Step 2 Homogenization of evolving microstructure

P

P

V

a_i n_j

Continuum after homogenizing the stationary microstructures

Fully homogenized continuum

Characterization of a damage entity
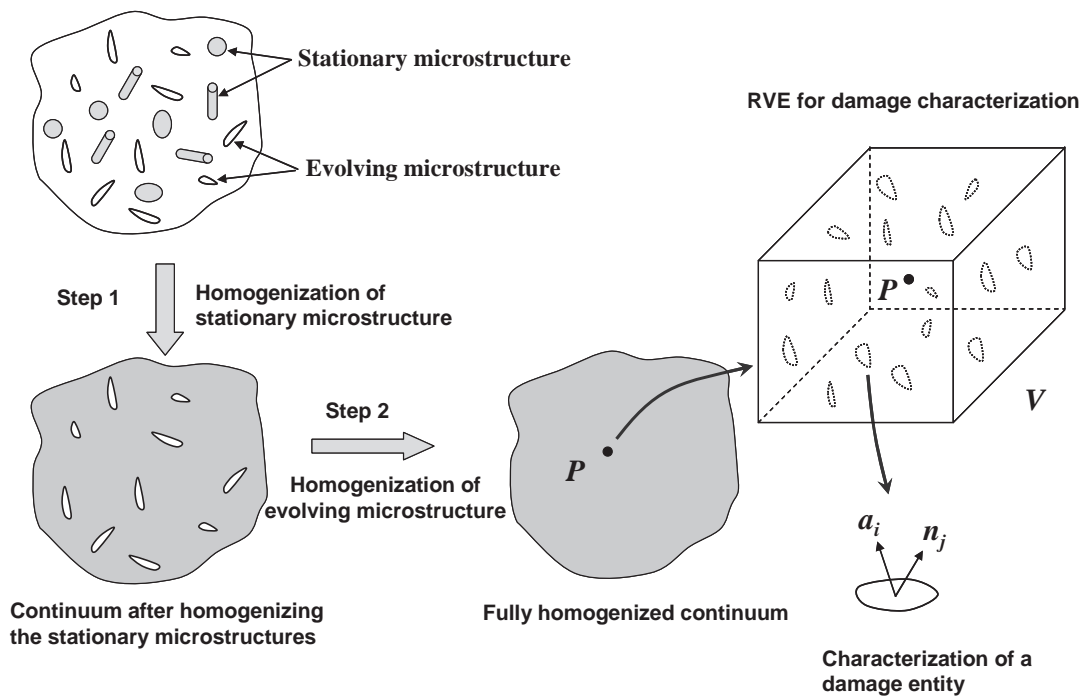
Figure 2. Homogenization of a continuum body with damage.

denoted by the second-order tensor components d_{ij}. Thus,

$$d_{ij} = \int_s a_i n_j \mathrm{d}S \qquad (1)$$

The total set of damage entities may be divided in subsets of entities having same geometrical characteristics (orientation, shape, etc.) and termed as damage modes. For example, matrix cracks may constitute one damage mode, while fibre/matrix debonds may constitute another. Also, matrix cracks in different orientations may be grouped into different damage modes. Assuming that there are N damage entities of a given mode α in the RVE, the damage mode tensor is defined by

$$D_{ij}^{(\alpha)} = \frac{1}{V} \sum_{k_\alpha} (d_{ij})_{k_\alpha} \qquad (2)$$

where $k_\alpha = 1, 2, \ldots, N$ and V is the volume of the RVE.

Let us now focus on the particular case of intralaminar cracking in composite laminates. Figure 3 shows an RVE illustrating one set of intralaminar cracks in an off-axis ply of a composite laminate. Although for clarity of illustration, the cracking is shown only in one lamina, it is understood that in general it exists in multiple plies of the laminate. The thickness of the cracked plies is denoted by t_c, s is the average crack spacing, t is the total laminate thickness and W and L stand for the width and the length, respectively, of the RVE. The volume of the RVE, the surface area of a crack, S, and the influence vector magnitude, a, are specified as

$$\begin{aligned} V &= L \cdot W \cdot t \\ S &= \frac{W \cdot t_c}{\sin \theta} \\ a &= \kappa t_c \end{aligned} \qquad (3)$$

where κ, called the constraint parameter, is an unspecified constant of (assumed) proportionality between a and the crack size t_c (also cracked-ply thickness). Here, $0 \le \theta \le \pi/2$, so that S is always positive. Assuming a to be constant over the crack surface S, one gets from equation (2)

$$D_{ij}^{(\alpha)} = \frac{\kappa t_c^2}{st \sin \theta} n_i n_j \qquad (4)$$

where $n_i = (\sin \theta, \ \cos \theta, \ 0)$.

The synergistic damage mechanics methodology

For the mechanical response of a damaged body in isothermal condition, the Helmholtz free energy function is given by[9]

$$\psi = \psi\left(\varepsilon_{ij}, D_{ij}^{(\alpha)}\right) \qquad (5)$$

Helmholtz free energy is thus a function of the damage state. The energy change brought about by damage is represented by terms involving $D_{ij}^{(\alpha)}$. The stress tensor is then given by

$$\sigma_{ij} = \rho_m \frac{\partial \psi}{\partial \varepsilon_{ij}} \qquad (6)$$

where ρ_m is the mass density.

For a linear elastic homogenized body,

$$\sigma_{ij} = C_{ijkl} \varepsilon_{kl} \qquad (7)$$

where the stiffness matrix C_{ijkl} is given in the Voigt notation as

$$\mathbf{C_{pq}} = \mathbf{C_{pq}^0} + \sum_\alpha \mathbf{C_{pq}^{(\alpha)}} \qquad (8)$$

where $\mathbf{C_{pq}^0}$ is the initial (undamaged) stiffness matrix and $\sum_\alpha \mathbf{C_{pq}^{(\alpha)}}$ represents the stiffness changes brought about by all the damage modes. In the following, we consider the different cases of cracking in composite laminates and derive the corresponding damage-stiffness relations.

Case 1: Only 90° ply is cracked (single damage mode). Let us consider the Helmholtz free energy for a composite laminate with its 90° ply cracked. As shown before,[8–10] a polynomial form is most suited for our formulation. Assuming the composite laminates in consideration to be orthotropic, the form of the polynomial must remain invariant with respect to the coordinate transformations expressing this symmetry. Such restrictions to polynomial functions are satisfied by making use of certain polynomial invariants called the irreducible integrity basis.[23,24] Considering a single damage mode, $\alpha = 1$, we have the following set of invariants

$$\begin{aligned} &\varepsilon_{11}, \varepsilon_{22}, \varepsilon_{33}, \varepsilon_{23}^2, \varepsilon_{31}^2, \varepsilon_{12}^2, \varepsilon_{23}\varepsilon_{31}\varepsilon_{12} \\ &D_{11}, D_{22}, D_{33}, D_{23}^2, D_{31}^2, D_{12}^2, D_{23}D_{31}D_{12} \\ &\varepsilon_{23}D_{23}, \varepsilon_{31}D_{31}, \varepsilon_{12}D_{12}, \\ &\varepsilon_{31}\varepsilon_{12}D_{23}, \varepsilon_{12}\varepsilon_{23}D_{31}, \varepsilon_{23}\varepsilon_{31}D_{12}, \\ &\varepsilon_{23}D_{31}D_{12}, \varepsilon_{31}D_{12}D_{23}, \varepsilon_{12}D_{23}D_{31} \end{aligned} \qquad (9)$$
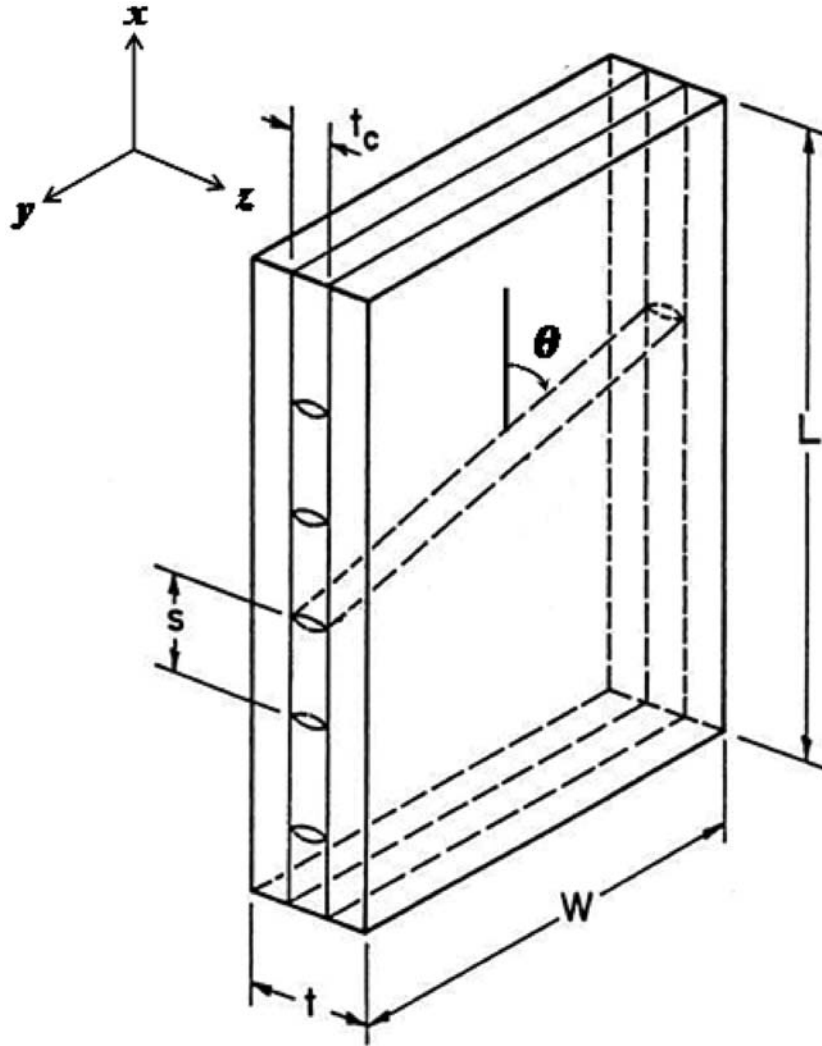
Figure 3. A representative volume element illustrating intralaminar multiple cracking in a general off-axis ply of a composite laminate.

This set of integrity bases can be further reduced for the case of a thin laminate loaded in its plane. For such laminates, only the in-plane transformed strain and damage tensor components need be considered. Thus, the remaining integrity bases in the Voigt notation for thin laminates are given by

$$\varepsilon_1, \varepsilon_2, \varepsilon_6^2$$
$$D_1, D_2, D_6^2$$
$$\varepsilon_6 D_6 \qquad (10)$$

where

$$\varepsilon_1 \equiv \varepsilon_{11}, \varepsilon_2 \equiv \varepsilon_{22}, \varepsilon_6 \equiv 2\varepsilon_{12}, D_1 \equiv D_{11}, D_2 \equiv D_{22}, D_6 \equiv D_{12}.$$

The most general polynomial form for Helmholtz free energy, restricted to second-order terms in the damage strain components and first order terms in damage tensor components (low volume fraction of damage entities), is given by

$$
\begin{aligned}
\rho\psi = P_0 &+ \left\{ c_1\varepsilon_1^2 + c_2\varepsilon_2^2 + c_3\varepsilon_6^2 + c_4\varepsilon_1\varepsilon_2 \right\} \\
&+ \left\{ c_5\varepsilon_1^2 D_1 + c_6\varepsilon_1^2 D_2 \right\} + \left\{ c_7\varepsilon_2^2 D_1 + c_8\varepsilon_2^2 D_2 \right\} \\
&+ \left\{ c_9\varepsilon_6^2 D_1 + c_{10}\varepsilon_6^2 D_2 \right\} + \left\{ c_{11}\varepsilon_1\varepsilon_2 D_1 + c_{12}\varepsilon_1\varepsilon_2 D_2 \right\} \\
&+ \left\{ c_{13}\varepsilon_1\varepsilon_6 D_6 + c_{14}\varepsilon_2\varepsilon_6 D_6 \right\} + P_1(\varepsilon_p, D_q) + P_2(D_q)
\end{aligned}
$$
$$(11)$$

where P_0 and c_i, $i = 1, 2, \ldots, 14$ are material constants, P_1 is a linear function of strain and damage tensor components and P_2 is a linear functions of damage tensor components. Setting the free energy to zero for unstrained and undamaged material, we have, $P_0 = 0$, and assuming the unstrained material of any damaged state to be stress-free, we get $\boldsymbol{P}_1 = 0$. The stress

components in the Voigt notation are now given by (from equation (6))

$$\sigma_p = \rho_m \frac{\partial \psi}{\partial \varepsilon_p} \tag{12}$$

where $p = 1,2,6$. From (11) and (12), we have

$$\mathbf{C_{pq}} = \mathbf{C_{pq}^0} + \mathbf{C_{pq}^{(1)}} \tag{13}$$

where $p, q = 1,2,6$, and

$$\mathbf{C_{pq}^0} = \begin{bmatrix} 2c_1 & c_4 & 0 \\ & 2c_2 & 0 \\ Symm & & 2c_3 \end{bmatrix}$$

$$= \begin{bmatrix} \dfrac{E_x^0}{1 - \nu_{xy}^0 \nu_{yx}^0} & \dfrac{\nu_{xy}^0 E_y^0}{1 - \nu_{xy}^0 \nu_{yx}^0} & 0 \\[2ex] & \dfrac{E_y^0}{1 - \nu_{xy}^0 \nu_{yx}^0} & 0 \\[2ex] Symm & & G_{xy}^0 \end{bmatrix} \tag{14}$$

represents the orthotropic stiffness matrix for virgin composite material, where $E_x^0, E_y^0, \nu_{xy}^0, G_{xy}^0$ are effective moduli for the undamaged laminate (calculated using CLT), and

$$\mathbf{C_{pq}^{(1)}} = \begin{bmatrix} 2c_5 D_1 + 2c_6 D_2 & c_{11}D_1 + c_{12}D_2 & c_{13}D_6 \\ & 2c_7 D_1 + 2c_8 D_2 & c_{14}D_6 \\ Symm & & 2c_9 D_1 + 2c_{10}D_2 \end{bmatrix} \tag{15}$$

represents the stiffness change brought about by the damage entities for damage mode 1. For the special case of laminates with cracks in only 90°-plies, we obtain ($\theta = 90°$)

$$\mathbf{C_{pq}^{(90)}} = \frac{\kappa t_c^2}{st} \begin{bmatrix} 2a_1 & a_4 & 0 \\ & 2a_2 & 0 \\ symm & & 2a_3 \end{bmatrix} \tag{16}$$

where $a_i, i = 1, \ldots, 4$ are material (laminate) constants to be determined from experimental or computational data on stiffness degradation. It can be observed that the orthotropic symmetry is retained by intralaminar cracking in cross-ply laminates. In the above relations, the constraint parameter $\kappa = \frac{\overline{(\Delta u_2)}}{t_c}$ where $\overline{(\Delta u_2)}$ and t_c represent the COD averaged over the crack surfaces

and the thickness of the cracked 90° layer, respectively. The engineering moduli for the cracked laminate can be obtained from the following relationships:

$$E_x = \frac{C_{11}C_{22} - C_{12}^2}{C_{22}} \quad E_y = \frac{C_{11}C_{22} - C_{12}^2}{C_{11}}$$

$$\nu_{xy} = \frac{C_{11}}{C_{22}} \qquad\qquad G_{xy} = C_{66} \tag{17}$$

Thus, for laminates with 90°-ply cracks only,

$$E_x = \frac{E_x^0}{1 - \nu_{xy}^0 \nu_{yx}^0} + 2\bar{D}a_1 - \frac{\left[\dfrac{\nu_{xy}^0 E_y^0}{1 - \nu_{xy}^0 \nu_{yx}^0} + \bar{D}a_4\right]^2}{\dfrac{E_y^0}{1 - \nu_{xy}^0 \nu_{yx}^0} + 2\bar{D}a_2}$$

$$E_y = \frac{E_y^0}{1 - \nu_{xy}^0 \nu_{yx}^0} + 2\bar{D}a_2 - \frac{\left[\dfrac{\nu_{xy}^0 E_y^0}{1 - \nu_{xy}^0 \nu_{yx}^0} + \bar{D}a_4\right]^2}{\dfrac{E_x^0}{1 - \nu_{xy}^0 \nu_{yx}^0} + 2\bar{D}a_1}$$

$$\nu_{xy} = \frac{\dfrac{\nu_{xy}^0 E_y^0}{1 - \nu_{xy}^0 \nu_{yx}^0} + \bar{D}a_4}{\dfrac{E_y^0}{1 - \nu_{xy}^0 \nu_{yx}^0} + 2\bar{D}a_2}$$

$$G_{xy} = G_{xy}^0 + 2\bar{D}a_3 \tag{18}$$

where

$$\bar{D} = \frac{\kappa t_c^2}{st} \tag{19}$$

As seen from equation (18), the shear modulus is uncoupled from the other three moduli and thus can be treated independently. The four constants appearing in these relations are evaluated by using initial elastic properties and their values at one crack spacing. Thus, if the chosen crack spacing is s_0, then

$$a_1 = \frac{1}{2\bar{D}_0}\left[\frac{E_x}{1 - \nu_{xy}\nu_{yx}} - \frac{E_x^0}{1 - \nu_{xy}^0 \nu_{yx}^0}\right]$$

$$a_2 = \frac{1}{2\bar{D}_0}\left[\frac{E_y}{1 - \nu_{xy}\nu_{yx}} - \frac{E_y^0}{1 - \nu_{xy}^0 \nu_{yx}^0}\right]$$

$$a_3 = \frac{1}{2\bar{D}_0}\left[G_{xy} - G_{xy}^0\right]$$

$$a_4 = \frac{1}{\bar{D}_0}\left[\frac{\nu_{xy}E_y}{1 - \nu_{xy}\nu_{yx}} - \frac{\nu_{xy}^0 E_y^0}{1 - \nu_{xy}^0 \nu_{yx}^0}\right] \tag{20}$$

with $\bar{D}_0 = \bar{D}\big|_{s=s_0} = \frac{\kappa t_c^2}{s_0 t}$.

Case 2: multiple damage modes. The details of damage modeling in multidirectional laminates with cracking in multiple off-axis plies are given in References [19–21] and reproduced in Appendix A for the sake of completeness. For the special case of $[0_m/90_r/\pm\theta_n]_s$ and $[0_m/\pm\theta_n/90_r]_s$ laminates with intralaminar cracks in $+\theta$, $-\theta$ and $90°$ layers, the stiffness-damage relations are same as in equation (18) except that $\bar{D}$ is now given by[18]

$$\bar{D} = \frac{2t_0^2}{t}\left[\frac{1}{s_n^\theta}\frac{\kappa_\theta}{\kappa_\theta|_{\theta=90}}\left\{2(2n+r)^2\kappa_{90_{4n+2r}} - r^2\kappa_{90}\right\} + r^2\frac{\kappa_{90}}{s^{90}}\right]$$

(21)

with the following constraint parameters

$$\kappa_\theta = \frac{(\overline{\Delta u_2})_{\pm\theta_{4n}}}{4nt_0}; \quad \kappa_{90_{4n+2r}} = \frac{(\overline{\Delta u_2})_{90_{4n+2r}}}{(4n+2r)t_0}; \quad \kappa_{90} = \frac{(\overline{\Delta u_2})_{90_r}}{rt_0}$$

(22)

for $[0_m/90_r/\pm\theta_n]_s$ laminates, and

$$\bar{D} = \frac{4t_0^2}{t}\left[\frac{1}{s_n^\theta}\frac{\kappa_\theta}{\kappa_\theta|_{\theta=90}}\left\{2(2n+r)^2\kappa_{90_{4n+2r}} - r^2\kappa_{90}\right\} + r^2\frac{\kappa_{90}}{s^{90}}\right]$$

(23)

with the following constraint parameters

$$\kappa_\theta = \frac{(\overline{\Delta u_2})_{\pm\theta_{2n}}}{2nt_0}; \quad \kappa_{90_{4n+2r}} = \frac{(\overline{\Delta u_2})_{90_{4n+2r}}}{(4n+2r)t_0}; \quad \kappa_{90} = \frac{(\overline{\Delta u_2})_{90_{2r}}}{2rt_0}$$

(24)

for $[0_m/\pm\theta_n/90_r]_s$ laminates, where t_0 is the thickness of a single ply, s_n^θ, and s^{90} are the normal crack spacings in $\pm\theta$ and $90°$-plies, respectively. In expressions for the constraint parameters, the subscript denotes a particular damage mode (orientation of cracked plies) and sub-subscript represents the number of cracked plies corresponding to that damage mode.

The flow chart in Figure 1 describes the procedure for multiscale synergistic methodology for multimode damage assessment taking an example of $[0_m/\pm\theta_n/90_r]_s$ laminates. Computational micromechanics involves analysis of a representative unit cell to determine the COD values and the constraint parameters. In a separate step, the material constants a_i appearing in equations (18) and (20) are determined from experiments or numerical simulations carried for a reference laminate, specifically $[0/90_3]_s$. These relations are then employed to predict stiffness degradation with constraint parameters and material constants obtained from experiments (or FE simulations) as inputs. In the final step, the overall structural behavior in response to external loading can be analyzed based on the degraded stiffness properties for the damaged laminate.

A reference laminate in principle could be any cross-ply laminate of a chosen configuration. The procedure for predicting cracking-induced property changes for other cross-ply laminates is independent of this choice. The specific choice of $[0/90_3]_s$ laminate was made here as experimental data for this laminate was available from which the constrained parameter could be estimated.

The procedure described above for determining elastic moduli changes in a laminate requires calculating CODs of ply cracks. However, the laminate elastic moduli can change additionally due to the nonlinear shear response of plies. In References [18,20] a procedure for correcting the CDM predictions by including this response was illustrated.

Modeling of damage evolution

For predicting evolution of ply cracking, the authors have developed an energy-based approach, which is capable of dealing with cracking in off-axis plies of orthotropic laminates. In Reference [25], the approach is described and applied to several ply cracking cases. Here, we apply it to the relevant WWFE-III test cases. A brief description of the approach follows.

As illustrated in Figure 4, two damage states are considered: State 1 with N parallel off-axis cracks spaced at distance s, and State 2 where the cracks have multiplied to $2N$ and attained spacing $s/2$. The crack density is assumed to increase when the work required in going from State 1 to State 2 (which is the

State 1: N cracks, crack spacing = s   State 2: 2N cracks, crack spacing = s/2
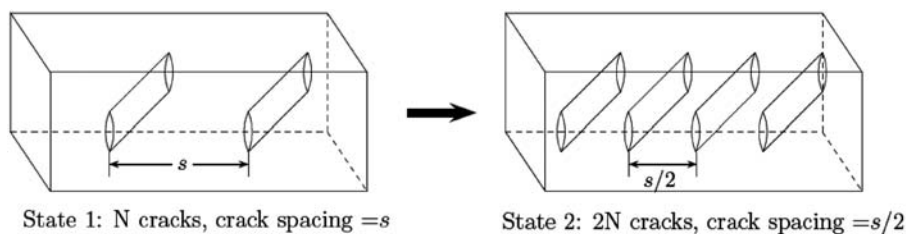
Figure 4. Progressive multiplication of intralaminar cracks in an off-axis ply.

same as work needed to close N cracks in going from State 2 to State 1) exceeds a critical value, i.e., if

$$W_{2N \to N} \geq N.G_c \frac{1}{\sin \theta} t_c \qquad (25)$$

where θ is the off-axis angle shown in Figure 3 and G_c is the critical (threshold) value of energy required for ply crack formation within the given laminate (more discussion about this later). The work required to form additional N cracks in going from State 1 to State 2 is therefore,

$$W_{2N \to N} = W_{2N \to 0} - W_{N \to 0} \qquad (26)$$

where $W_{N \to 0}$ and $W_{2N \to 0}$ represent work required to close N cracks in State 1, and $2N$ cracks in State 2, respectively, and the two quantities are calculated as (see Reference [21] for detailed derivation)

$$W_{N \to 0} = N \frac{1}{\sin \theta} (t_c)^2 \cdot \frac{1}{E_2} \left[(\sigma_{20}^\theta)^2 . \tilde{u}_n^\theta(s) + (\sigma_{120}^\theta)^2 \cdot \tilde{u}_n^\theta(s) \right] \qquad (27)$$

$$W_{2N \to 0} = 2N \frac{1}{\sin \theta} (t_c)^2 \cdot \frac{1}{E_2} \left[(\sigma_{20}^\theta) . \tilde{u}_n^\theta \left(\frac{s}{2}\right) + (\sigma_{120}^\theta)^2 \cdot \tilde{u}_t^\theta \left(\frac{s}{2}\right) \right] \qquad (28)$$

where $\tilde{u}_n^\theta$, $\tilde{u}_t^\theta$ are the normalized average crack opening and sliding displacements (COD and CSD). These are given by

$$\tilde{u}_n^\theta = \frac{\bar{u}_n^\theta}{t_c (\sigma_{20}^\theta / E_2)} = \frac{1}{t_c^2 (\sigma_{20}^\theta / E_2)} \int_{-t_c/2}^{t_2/2} u_n(z) \mathrm{d}z$$

$$\tilde{u}_t^\theta = \frac{\bar{u}_t^\theta}{t_c (\sigma_{120}^\theta / E_2)} = \frac{1}{t_c^2 (\sigma_{120}^\theta / E_2)} \int_{-t_c/2}^{t_2/2} u_t(z) \mathrm{d}z \quad (29)$$

where u_n and u_t represent the relative opening and sliding displacement of the cracked surfaces, respectively, and overbars represent averages. For the special case of cracking in 90°-ply only, the sliding displacement is zero (under uniaxial loading condition) and hence the criterion for ply multiplication is written as

$$t_c \frac{(\sigma_{20}^\theta)}{E_2} \left[2.\tilde{u}_n^\theta \left(\frac{s}{2}\right) - \tilde{u}_n^\theta(s) \right] \geq G_{Ic} \qquad (30)$$

where G_{Ic} is the critical energy release rate in Mode I (crack opening mode). This is the same relation as derived for cracking in cross-ply laminates by Joffe et al.[26] except that they consider centrally placed cracked 90°-plies in their model and normalize the average COD with half the ply thickness ($t_c/2$). For cracking

in a general off-axis ply, one can use a multimode criterion given as

$$\left(\frac{w_I}{G_{Ic}} \right)^M + \left(\frac{w_{II}}{G_{IIc}} \right)^N \geq 1 \qquad (31)$$

where

$$w_I = \frac{(\sigma_{20}^\theta)^2}{E_2} \left[2.\tilde{u}_n^\theta \left(\frac{s}{2}\right) - \tilde{u}_n^\theta(s) \right];$$

$$w_{II} = \frac{(\sigma_{120}^\theta)^2 t_c}{E_2} \left[2.\tilde{u}_t^\theta \left(\frac{s}{2}\right) - \tilde{u}_t^\theta(s) \right] \qquad (32)$$

and G_{IIc} is the critical energy release rate in Mode II (crack sliding mode), and the exponents M and N depend on the material system, for example, for glass/epoxy $M = 1$, $N = 2$.[35]

In our work,[25] we interpret the critical material parameters G_{IC} and G_{IIC} not in the usual linear elastic fracture mechanics sense where they are defined as the resistance to advancement of the crack front at the point of unstable crack growth. Instead, we postulate that the work required to go from State 1 to State 2 involves a range of dissipative processes that all depend on the material condition in a cracking ply within the given laminate. The material parameter representing the dissipated energy per unit of ply crack surface is, therefore, not what is obtained in a standard fracture toughness test for determining G_{Ic} or G_{IIc}. Furthermore, as discussed in Reference [25], we believe a ply crack cannot form unless sufficient energy is available to open its surfaces (i.e. mode I). In other words, a pure sliding action will not generate a set of parallel cracks illustrated in Figure 4. This will imply that the second term in equation (31) is negligible. In fact, we report good predictions of crack density evolution by only using the first term in equation (31). Also, we do not use the conventional G_{Ic} but extract this value from test data of a reference laminate and use it to make predictions for other laminates. For the WWFE-III, however, we are given conventional G_{Ic} and G_{IIc} and have used those. Thus, the predictions reported here will not be in accordance with our analysis proposed in Reference [25].

Analysis method

The prediction of overall stress–strain response for a given damaged laminate using CDM entails following steps:

1. Determine damage constants a_i that appear in the damage-stiffness relations (equation (18), using equation (20)). This task requires stiffness constants

for virgin (undamaged) laminate, E_x^0, E_y^0, G_{xy}^0, v_{xy}^0, and moduli of cracked laminates at some specified crack spacing, s_0 : $E_x(s_0)$, $E_y(s_0)$, $G_{xy}(s_0)$, $v_{xy}(s_0)$. The moduli for virgin laminate are obtained through the classical laminated plate theory (CLT) by using the properties of a unidirectional lamina, whereas their values at crack spacing s_0 are obtained by micromechanical analysis using finite element method (FEM) for reference laminate $[0/90_3]_s$. In earlier works, e.g., References [18,20], these constants were obtained using experimental data for stiffness changes. It is noted here that the choice of a reference laminate is driven by convenience and availability of experimental data. Since in earlier works[18,20] the $[0/90_3]_s$ laminate was used to obtain the material constants, the same laminate was then used in later work as the reference laminate for FEM calculations.

2. Find stiffness constants as a function of crack density ($\rho_c = 1/s$) using equation (18), depending on the laminate type. This gives,

$$C_{ijkl} = f_1(\rho_c) \tag{33}$$

3. Predict evolution of crack density as a function of applied axial strain using the fracture criterion expressed in equation (30). Thus,

$$\rho_c = f_2(\varepsilon_{ij}) \tag{34}$$

The strain to initiation of first multiple cracking can be estimated by backward extrapolation of the function f_2.

4. Combine results from steps 2 and 3 (equations (33)–(34)) to obtain stiffness properties as a function of applied strain, equation (35), and predict the overall stress–strain response of the laminate for axial tensile loading along laminate longitudinal direction.

$$C_{ijkl} = c_{ijkl}(\varepsilon_{ij}) \tag{35}$$

Computational micromechanics (FE analysis). As described above, SDM approach requires evaluation of COD and damage constants, experimentally or computationally. Since the BVP for multidirectional laminates is inherently three-dimensional, we use 3D FE analysis to compute these parameters. For the reference cross-ply laminate, the representative unit cell is as shown in Figure 5. For this laminate layup, periodic boundary conditions are applied to the end faces in the transverse (y) direction, and laminate symmetry about the mid-plane is achieved by having out-of-plane displacements (w) zero at the symmetry plane. Uniform displacement is prescribed on the right face of the cell to have tensile loading. However, for multidirectional laminates with cracks in more than two orientations (e.g. multimode cracking in $[0/90/+\theta/-\theta]$ laminates), the construction of FE model is somewhat complex and is detailed in References [21,25]. For SDM predictions for laminates, we chose $[0/90_3]_s$, i.e. $\theta = 90°$, as a reference laminate. The stiffness–damage results for this cross-ply laminate can be obtained in a variety of ways. The most obvious way would be by using experimental data. However, although experiments reflect the real material behaviour, they can be performed for limited cases. An alternative and more general way is to use a numerical tool such as an FE model to simulate stiffness degradation. FE simulations are in fact easier to carry out and have no scatter other than the accuracy of computations that may depend on mesh density and implementation of boundary conditions. The crack density along x direction (or equivalently, the crack spacing) was varied by changing the length of the unit cell considered. Linear elastic FE analyses were carried using ANSYS 11[27] for the reference laminate. The cracks were assumed to be fully grown through thickness and width of 90°-plies. The longitudinal modulus and the Poisson's ratio of the damaged laminate were obtained using the volume averaging[28] of stresses and strains as given by
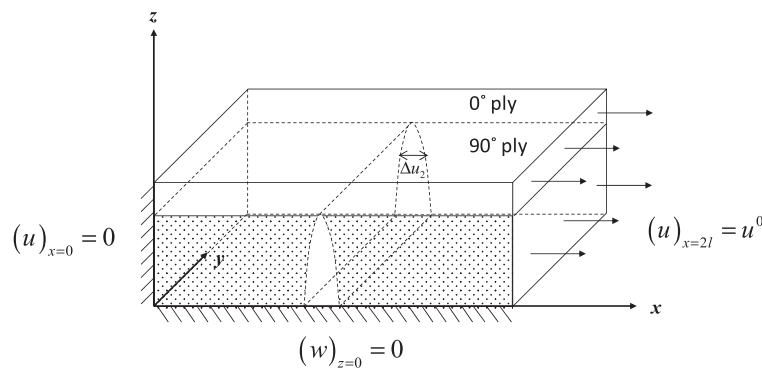
Figure 5. Representative unit cell for FE analysis of reference $[0/90_3]_s$ laminate. The applied displacement boundary conditions are shown above. Periodic boundary conditions are applied on end faces in the width (y) direction.

the following equations

$$E_x = \frac{\langle \sigma_{xx} \rangle}{\langle \varepsilon_{xx} \rangle} \qquad (36)$$

$$v_{xy} = -\frac{\langle \varepsilon_{yy} \rangle}{\langle \varepsilon_{xx} \rangle} \qquad (37)$$

where brackets $<>$ specify volume averaging. CODs averaged over thickness of the cracked ply are calculated from

$$\overline{\Delta u_2} = \frac{1}{t_c} \int_{-t_c/2}^{t_c/2} \Delta u_2(z)\, \mathrm{d}z \qquad (38)$$

where $\Delta u_2 = u_2^+ - u_2^-$ represents the separation of crack planes in the direction normal to the crack face in the local lamina coordinate system x_1, x_2, x_3 with x_1 along crack longitude, x_2 transverse to the crack and x_3 along ply thickness. Numerically, Δu_2 is determined from nodal x_2-direction displacements averaged over the entire crack surface. The above micromechanical expressions are exact in the sense that they do not involve any homogenization theory and are directly calculated from FE data. Errors in the calculations can be only due to approximation in FE analysis. Further details on FE analysis methodology and validation for multidirectional laminates can be found in References [20,21,25,29,30].

It should be pointed out here that we have not included thermal stresses caused by cooling down of the composite laminates to the room temperature. However, it can be easily taken into account during prediction of damage evolution by including thermal stresses, which are calculated here by classical laminate plate theory (CLT). We demonstrate the effect of thermal stresses on one of the test cases: Test case 4. The coefficient of thermal expansion is assumed to be constant during entire loading process. Hence, we neglect any change in thermal expansion brought about by ply cracking.

Theoretical prediction of the WWFE-III test cases

The SDM model, by itself, is limited to the prediction of effect of sub-critical damage (matrix cracking, for the present scenario) on the stiffness properties of the laminated structure. Unlike the lamina failure theories, it cannot predict the lamina or laminate failure. Hence, our analysis here is limited to the test cases where effect of damage on the stress–strain response is desired. The test cases, thus analyzed are Test Case 3, Test Case 4, Test Case 6, Test Case 7, Test Case 8, Test Case 12 and Test Case 13. The input data for the analysis performed here is taken from Reference [31].

In the first step, we carried out FE simulations to characterize stiffness properties for reference laminate $[0/90_3]_s$ for all material types. Thickness of a single ply is taken as 0.125 mm. The crack density for these calculations in simulations was taken to be equal to 1.0 cr/mm. Axial tensile loading along laminate longitude was applied to the representative unit cell shown in Figure 5. The changes are thus assumed to occur only in E_x, and v_{xy}, where as E_y and G_{xy} are assumed to be impervious to damage for this laminate layup. The relative stiffness properties, constraint parameters, $\bar{D}_0$, and the corresponding damage constants for three material systems, viz. Glass/epoxy1 (Glass/LY556), $G4 - 800/5260$ and IM7/8552 targeted in this study, are shown in Table 1.

These constants were assumed to be the same for different test cases as long as the ply material remains the same. To evaluate the stiffness changes for various test layups, the constraint parameters were obtained in each case for crack density equal to 0.1 cr/mm (see Tables 2 and 3 for calculated COD values for different test cases). Then using expressions in equation (18), stiffness properties for other laminates were obtained. In doing so, it must be emphasized that since the damage constants are laminate-dependent, they must be adjusted in case the thickness of the cracked ply in the laminate configuration changes, e.g., for Test

Table 1. Stiffness properties and constraint parameters for reference $[0/90_3]_s$ laminates made for different materials. The relative stiffness changes are determined from FE simulations at crack density equal to 1 cr/mm, whereas the constraint parameters are calculated at an assumed initial crack density equal of 0.1 cr/mm

Material type	Constraint parameter, κ	$\bar{D}_0$	E_x/E_x^0	v_{xy}/v_{xy}^0	Damage constants, a_i (GPa)			
					a_1	a_2	a_3	a_4
Glass/epoxy1 (Glass/LY556)	7.61e-3	4.28e-3	0.631	0.457	−1070.8	−69.7	0	−594.7
G4-800/5260	5.65e-3	3.18e-3	0.898	0.483	−828.3	−25.3	0	−541.8
IM7/8552	5.78e-3	3.25e-3	0.903	0.478	−729.8	−22.6	0	−496.0

Case 4: $[0/90_4]_s$ laminate,

$$a_1' = a_1 \frac{(C_{11}^0)_{[0/90_4]_s}}{(C_{11}^0)_{[0/90_3]_s}}; \quad a_1' = a_2 \frac{(C_{22}^0)_{[0/90_4]_s}}{(C_{22}^0)_{[0/90_3]_s}};$$

$$a_3' = a_3 \frac{(C_{66}^0)_{[0/90_4]_s}}{(C_{66}^0)_{[0/90_3]_s}}; \quad a_4' = a_4 \frac{(C_{12}^0)_{[0/90_4]_s}}{(C_{12}^0)_{[0/90_3]_s}} \quad (39)$$

where a_i' represents re-evaluated constants for the laminate in consideration and a_i represents constants for the reference laminate. Thus, the constants a_is are re-calculated every time the relative thickness of layers in the laminate changes.

To simulate the stress–strain response, we need damage evolution predictions. For this purpose, an

Table 2. Calculated average COD values for 90° cracking for selected test cases. All COD values are in μm

Crack density (1/mm)	Test Case 3	Test Case 4	Test Case 6	Test Case 7	Test Case 8
0.1	0.770	7.986	2.884	1.706	0.700
0.2	0.765	7.303	2.850	1.703	0.702
0.3	0.763	6.728	2.817	1.697	0.704
0.4	0.762	6.241	2.782	1.689	0.709
0.5	0.760	5.812	2.741	1.682	0.717
0.6	0.758	5.408	2.689	1.669	0.722
0.7	0.757	5.015	2.632	1.656	0.725
0.8	0.755	4.638	2.565	1.639	0.724
0.9	0.754	4.290	2.490	1.620	0.720
1.0	0.752	3.975	2.409	1.603	0.718
1.1	0.750	3.694	2.333	1.586	0.715
1.2	0.748	3.443	2.248	1.566	0.711
1.3	0.747	3.222	2.171	1.551	0.711
1.4	0.746	3.023	2.094	1.529	0.706
1.5	0.743	2.848	2.013	1.511	0.706
1.6	0.742	2.690	1.941	1.487	0.701
1.7	0.741	2.550	1.871	1.466	0.701
1.8	0.739	2.423	1.804	1.439	0.695
1.9	0.736	2.308	1.741	1.418	0.695
2.0	0.733	2.202	1.675	1.395	0.695

COD: crack opening displacement.

Table 3. Calculated average COD values for 90° cracking for Test Cases 12 and 13. All COD values are in μm

Crack density (1/mm)	Test Case 12	Test Case 13, $m = 1$	Test Case 13, $m = 2$	Test Case 13, $m = 3$
0.2	3.223	0.770	1.680	2.424
0.4	2.982	0.739	1.611	2.330
0.6	2.832	0.712	1.553	2.204
0.8	2.686	0.683	1.491	2.124
1.0	2.531	0.664	1.448	2.051
1.2	2.381	0.649	1.416	1.967
1.4	2.209	0.633	1.381	1.872
1.6	2.059	0.615	1.343	1.786
1.8	1.917	0.601	1.311	1.686
2.0	1.731	0.580	1.266	1.600

COD: crack opening displacement.
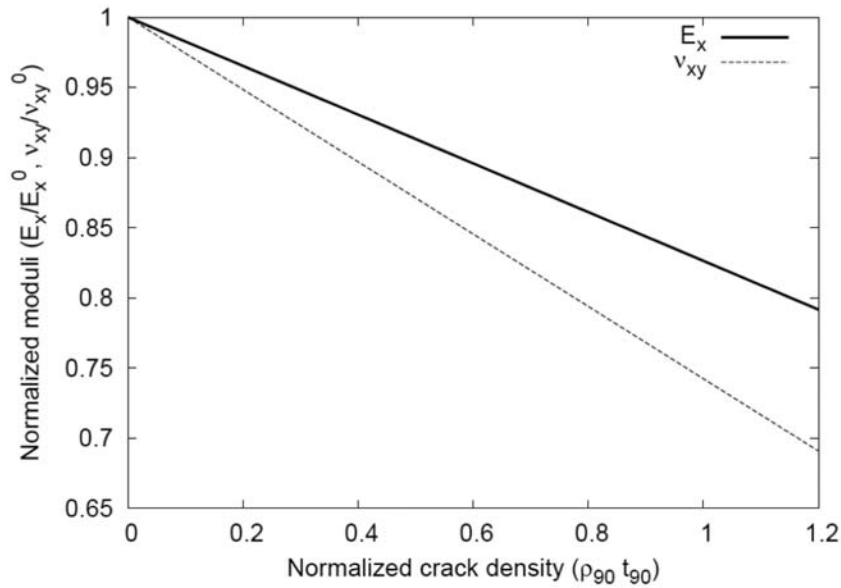
Figure 6. Stiffness and Poisson's ratio degradation for Test Case 3: $[0/90/0]_T$ glass/epoxy1 laminate.
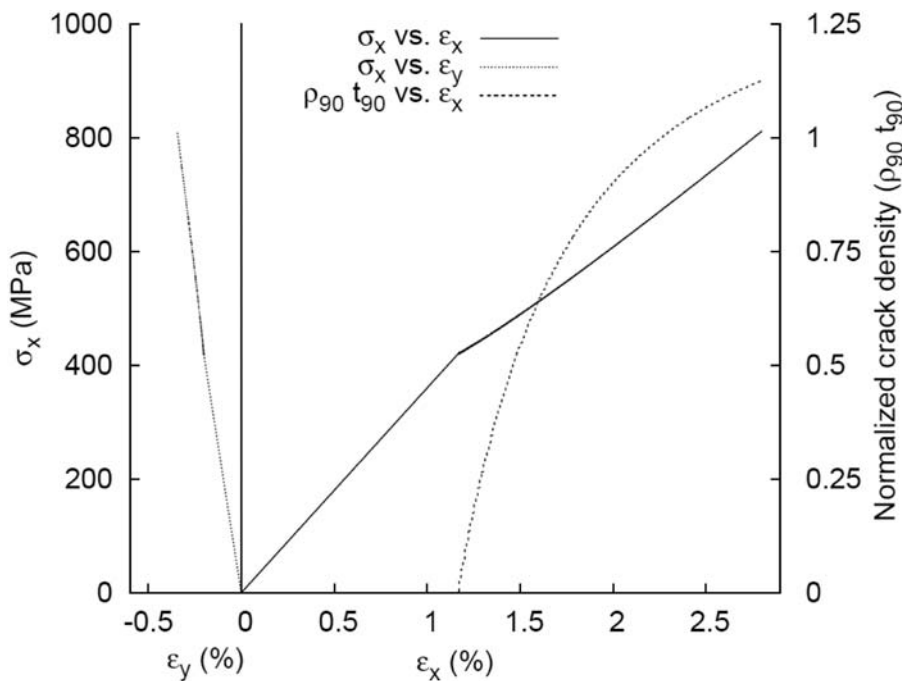
Figure 7. Stress–strain response and crack density evolution for Test Case 3: $[0/90/0]_T$ glass/epoxy1 laminate. No thermal effects were taken into account.

energy-based fracture criterion given in equation (30) was utilized in a MATLAB code. The normalized average COD and CSD for different crack spacing were obtained using FE simulations on the representative unit cell for the respective laminate. For 90° cracking, the calculated COD values are tabulated in Table 2 (CSD = 0 for 90°-cracks). Polynomial fits to these

COD values were used in the simulation for damage evolution. The damage evolution subroutine was run until the applied strain reaches longitudinal failure strain in tension. If the calculated crack initiation strain comes out to be higher than the longitudinal failure strain, the laminate is understood to have failed by fibre fractures.
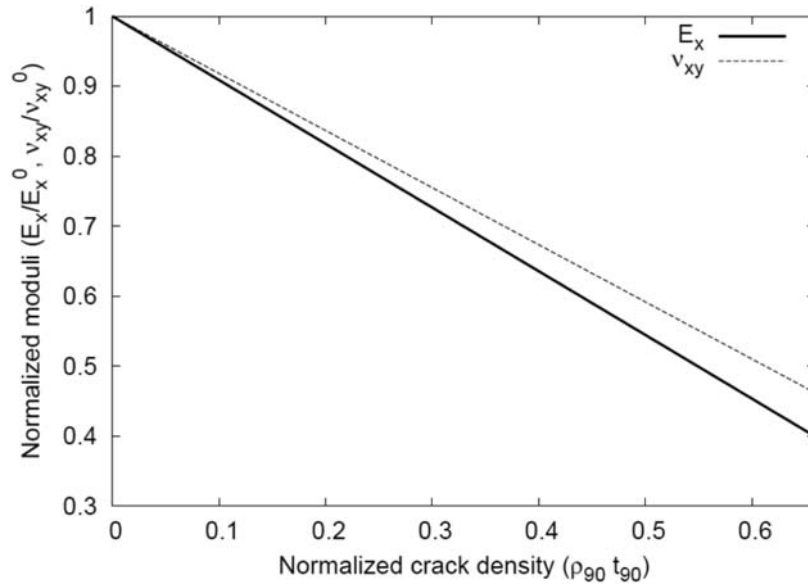
Figure 8. Stiffness and Poisson's ratio degradation for Test Case 4 $[0/90_8/0]_T$ glass/epoxy1 laminate.

For stiffness changes, the damage model considered in the present study is a linear model with respect to the crack density. A nonlinear model will involve additional damage constants and would be required to achieve a better accuracy for high crack density. For present purpose of illustration, a linear approach is sufficient.

Test Case 3. For this test case, Figure 6 shows the variation of longitudinal Young's modulus and the Poisson's ratio normalized with initial values $\left(\frac{E_x}{E_x^0}, \frac{v_{xy}}{v_{xy}^0}\right)$ against the normalized crack density ($\rho_{90}t_{90}$). The evolution of crack density and corresponding stress–strain response are shown in Figure 7. For this laminate case, the ply cracks initiate in 90°-plies at an applied axial strain of about 1.2%. After initiation, cracks grow in number very quickly on increase in applied strain and reach a saturation level subsequently. The overall shape of crack density increase is parabolic. The value of $\rho_{90}t_{90}$ reached at longitudinal tensile failure strain ($\varepsilon_{1T} = 2.807\%$) for this material is slightly more than 1.0, suggesting a very high value of absolute crack density ($\sim$8 cracks/mm). Still the effect on stress–strain response is not too severe as would be for thicker 90°-plies (such as in the next Test Case). Although the Poisson's ratio reduces, its effect on the transverse stress–strain curve (σ_x vs. ε_y) is almost negligible.

Test Case 4. For this test case, the laminate material is same as in the previous one. However, the thickness of the 90°-plies is eight times of that in the previous case. Consequently, the degradation in the laminate stiffness due to ply cracking is much more severe in the present

case (see Figure 8). Also, the ply cracks in 90°-plies initiate at much lower applied strain of about 0.37%. As compared to the Test Case 3, however, the rate of damage evolution is lower in this case and the value of $\rho_{90}t_{90}$ reached at $\varepsilon_x = \varepsilon_{1T}$ for this material is 0.66, suggesting much lower absolute crack density (0.66 cracks/mm). The shape of the damage evolution curve is quite similar to that in Test Case 3 (Figure 9). The stress–strain response (also in Figure 9) is significantly nonlinear after ply cracking. For thicker cracked plies, thus, ply cracking may cause severe nonlinearity in the longitudinal stress–strain response. Although there is large reduction in the Poisson's ratio subsequent to ply cracking, its effect on the transverse stress–strain curve (σ_x vs. ε_y) is not visible.

Here, we also illustrate the effect of thermal residual stresses on ply cracking and the resultant stress–strain response. Due to differential thermal expansion of longitudinal and transverse plies, the inner 90°-ply will develop compressive thermal residual strains when it is cooled from curing to the room temperature. The residual thermal strains due to thermal effects during curing are calculated using CLT as[32]

$$
\begin{aligned}
\varepsilon^{th} &= \frac{t_0 E_1}{t_0 E_1 + t_{90} E_2} \left(\alpha_2 - \alpha_1\right) \Delta T \\
&= \frac{45.6}{4 * 16.2 + 45.6} * (26.4 - 8.6) * 10^{-6} * (120 - 25) \\
&= 6.98 * 10^{-4} \approx 0.07\%
\end{aligned}
$$

(40)

where t_0 is 0° ply thickness, and $\Delta T = T_{\text{ref}} - T_{\text{service}}$ with $T_{\text{service}} = 25°C$ being the service (room)
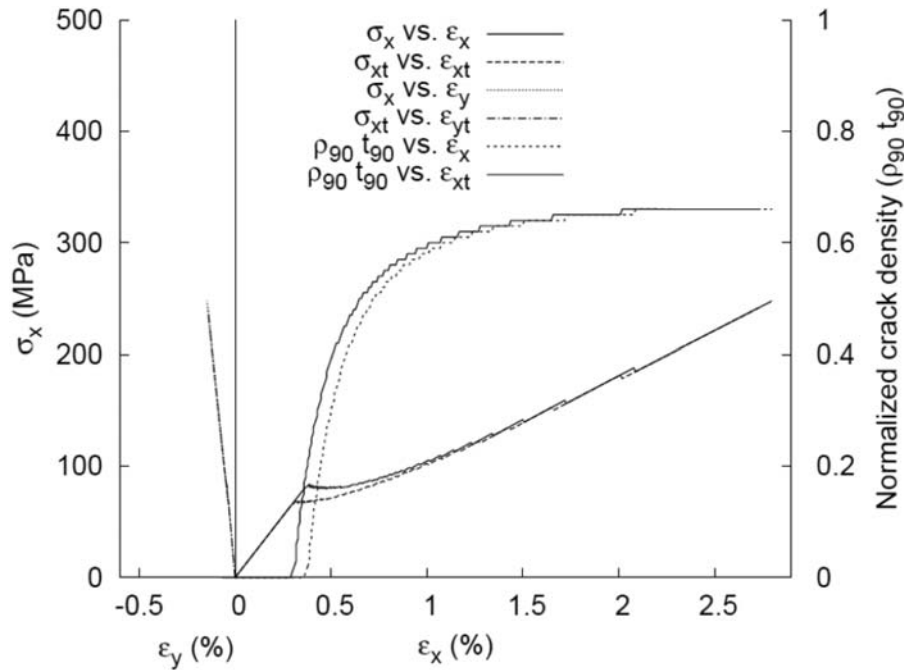
Figure 9. Stress–strain response and crack density evolution for Test Case 4: $[0/90_8/0]_T$ glass/epoxy1 laminate. Dashed lines (denoted in legend by second subscript *t*) include the effect of strains generated due to thermal mismatch between $0°$ and $90°$-plies during curing on damage initiation and progression.

temperature, $T_{ref} = 120°C$ being the curing (stress free) temperature. The crack initiation strain thus decreases by 0.07% from the earlier value obtained without considering thermal effects. The rate of damage progression is however independent of thermal residual stresses. Thus, the new damage evolution curve just gets shifted to the left of the curve without such effects by an amount equal to thermal residual strain. The stress–strain response is also affected as shown in Figure 9 by dashed lines (using second subscript *t* in legend). Thermal effects are observed to be small for transverse stress–strain response.

Test Case 6. For multidirectional laminates, the damage will form in multiple plies of different orientations. For the specific case of quasi-isotropic laminates considered here in Test Cases 6–8, the cracks may form in $90°$, $+45°$ and $-45°$ layers. The combined effect of these cracks is felt more severely on the overall stiffness properties. Although most of stiffness degradation comes from $90°$ cracks, $\pm45°$ cracks may interact with $90°$ cracks and cause more severe degradation than what would be observed if cracks in these different damage modes occurred without affecting each other. SDM model is capable of dealing with this multimode damage scenario, as depicted by stiffness-damage relationships with $\bar{D}$ described in equations (21)–(24). Obviously, the density and opening displacements of intralaminar cracks in a given layer will depend on

the material, orientation and the thickness of that ply and also on the relative constraint on the cracked ply from surrounding supporting plies. For oblique cracks, sliding of the cracked surfaces will also play a role in the cracking criterion according to equation (31). It is often observed in experiments, for example Reference [30], that $\pm45°$ cracks may not grow fully before the laminate fails by delamination, and therefore we will assume $\pm45°$ cracks are half-developed, i.e. while evaluating stiffness properties we will reduce the total crack density $\pm45°$ such that the effective crack density in these plies is given by $(\rho_{45})_{eff} = \rho_r \rho_{45}$; $\rho_r = 0.5$. More detailed information about the growth of cracks is necessary to model this behaviour. This relative density is chosen for illustration purpose only and is based on our experience with model's usage to predict stiffness degradation in quasi-isotropic laminates[21] for experimental data on quasi-isotropic laminates reported in Reference [33]. The respective crack densities in different cracked plies are obtained using the damage progression model. Actual experimental observations may be necessary to simulate real material behaviour more accurately. The resulting plots for longitudinal Young's modulus and Poisson's ratio for Test Cases 6, predicted using expressions in equations (18) and (21), are shown in Figure 10. The constraint parameters for $\pm45°$ cracking with respect to that for $90°$ cracking are calculated using the parametric equation developed for COD variation with respect to ply orientation in Reference [20]
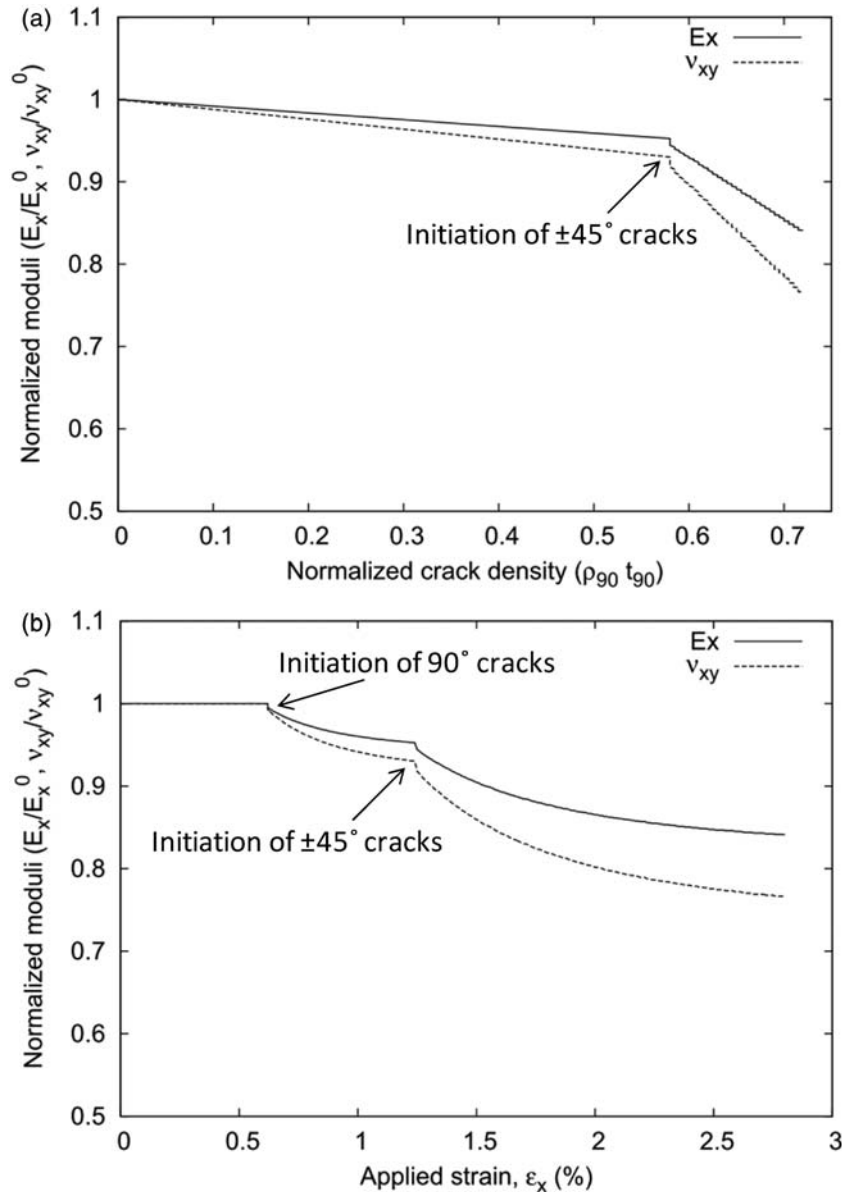
Figure 10. Variation of longitudinal Young's modulus and Poisson's ratio: (a) vs. normalized crack density in 90° ply and (b) vs. applied strain for Test Case 6: $[0/90/-45/+45]_s$ glass/epoxy1 laminate. Cracks in all off-axis modes are accounted depending on their respective initiation strains and variation of crack densities with applied strain as shown in the next figure. No thermal effects were taken into account.

considering cracking in $\pm\theta$ cracking in $[0/\pm\theta/0_{1/2}]_s$ Glass/epoxy1 laminates:

$$(\overline{\Delta u_2})_\theta = (\overline{\Delta u_2})_{90} \sin^2 \theta \qquad (41)$$

Also, it is assumed that $\kappa_{90_{4n+2r}} = \kappa_{90}$ and $\kappa_\theta|_{\theta=90} = \kappa_{90}$. It is noted that the above equation may not be accurate when cracks in multiple off-axis orientations are present with different crack densities. A more detailed FE computation with experimentally observed crack densities is warranted in such a case.

The COD variation in $\pm 45°$ plies is assumed following equation (41). As a simplification, the cracking in both $\pm 45°$ plies is assumed to initiate at identical applied strain and progress with same rate, although experiments may suggest that the 45° ply that is adjacent to 90° ply may fail earlier.[33] In Figure 10, we first show the variation of laminate stiffnesses with respect to crack density in 90° ply. Because at higher applied strains cracks are present in all off-axis orientations, Figure 10(b) is more appropriate, which shows their variation with respect to the applied strain. The damage progression in all off-axis plies is shown in
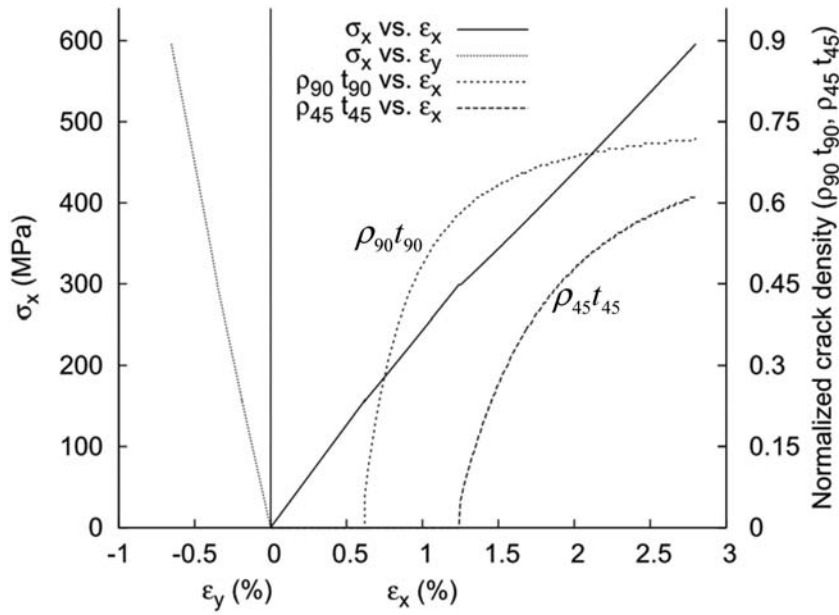
Figure 11. Stress–strain response and crack density evolution for Test Case 6: $[0/90/-45/+45]_s$ glass/epoxy1 laminate with cracks in all off-axis modes. The crack initiation and the crack density evolution in both $45°$ plies are assumed to be identical. No thermal effects were taken into account.
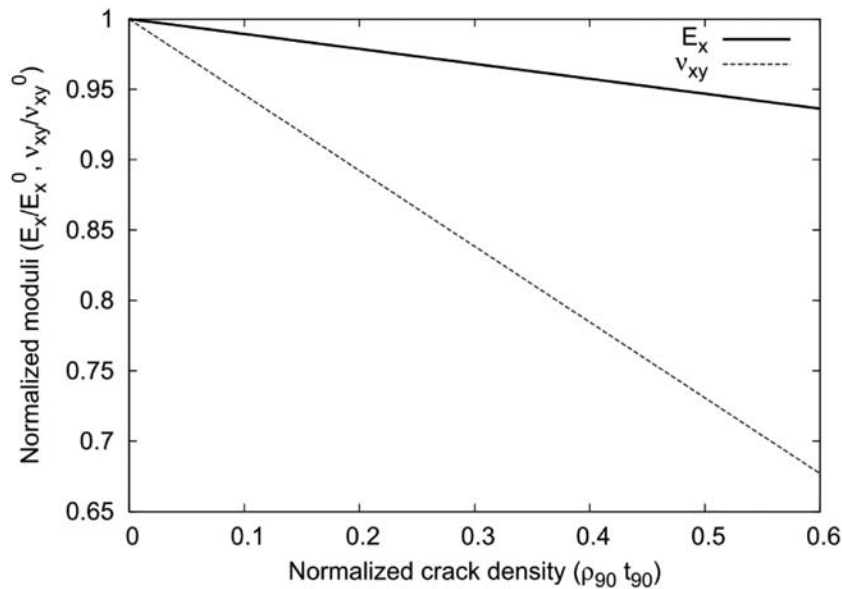
Figure 12. Stiffness and Poisson's ratio degradation for Test Case 7: $[0/-45/+45/90]_s$ $G4-800/5200$ laminate.

Figure 11. The cracks initiate in $90°$ ply at about 0.62% axial strain, and in $\pm45°$ plies at about 1.25% axial strain. Initial stiffness degradation ($\varepsilon_x > 0.62\%$) occurs due to $90°$ cracks only, whereas later ($\varepsilon_x > 1.25\%$) $45°$ cracks also contribute to stiffness degradation. The evolution curves for normalized crack densities in $95°$ and $45°$ plies have similar shapes, with saturation levels of $\rho_{90}t_{90} \approx 0.72$; $\rho_{45}t_{45} \approx 0.6$. No thermal effects were

considered while predicting damage progression and resultant stiffness properties.

As a result of ply cracking in multiple orientations, the stiffness degradation is more severe than would be for cracking in $90°$-plies only. As reported in Reference [33], cracks in $\pm45°$ plies will typically form from 45/90 interfaces and tend to further enhance opening of cracks present in $90°$-plies. This increases the rate of
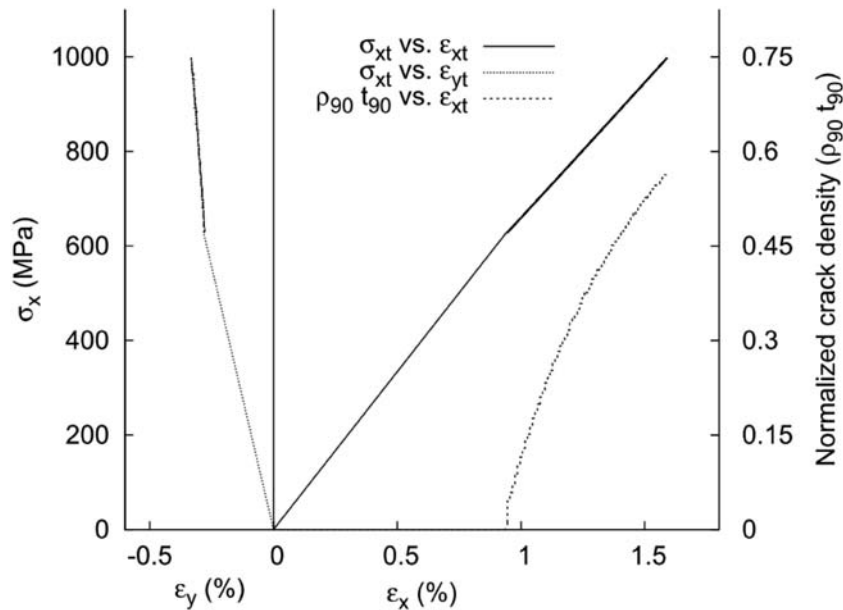
Figure 13. Stress–strain response and crack density evolution for Test Case 7: [0/−45/+45/90]$_s$ G4 − 800/5200 laminate with cracks in 90°-plies only. Strains generated due to thermal mismatch between 45°- and 90°-plies during curing were taken into account while evaluating damage initiation and progression.

damage evolution as well as corresponding degradation in stiffness properties and is not accounted for here. Some nonlinearity is observed in longitudinal and transverse stress–strain curves (Figure 11).

Test Case 7. For this ply material, we observed that our FE calculations on reference laminate [0/90$_3$]$_s$ showed very small relative degradation in E_x but significant degradation in v_{xy} (see Table 1). The COD, hence the constraint parameter, was also calculated to be smaller with this material. Therefore, the changes in longitudinal Young's modulus are less pronounced for laminate with this material than Glass/epoxy1. Figure 12 shows the predicted changes in stiffness properties for this case. The corresponding stress–strain response along with crack density evolution is shown in Figure 13.

For laminates made from G4-800/5260 material, thermal residual stresses generated during curing were found to affect the damage initiation behaviour significantly. For the present layup [0/−45/+45/90]$_s$, the mismatch in axial thermal strains between the 45° and the 90°-plies during curing is calculated as 0.311%. This decreases the crack initiation strain in 90°-plies to about 0.9% (Figure 13). The model does not predict any cracking in 45° plies. The shape of crack density evolution is about the same as before with maximum normalized crack density in 90°-plies at about 0.6 at $\varepsilon_x = \varepsilon_{1T}$. Appreciable nonlinearity is seen in stress–strain responses, especially the transverse stress–strain response.

Test Case 8. When only mechanical strains were considered, our model did not predict any cracking for this laminate (i.e. crack initiation strain for this case was determined to be greater than the provided failure strain for unidirectional lamina). However, when we include residual thermal strains, the cracking in 90°-plies is predicted. The reduction in the longitudinal stiffness and Poisson's ratio is predicted to be similar to Test Case 7 (Figure 14) when absolute crack densities are considered. However, the crack initiation and progression behaviour (Figure 15) is quite different mainly due to different thicknesses of 90°-plies in the two test cases. For the present case, the mismatch between 0° and 90°-plies is important, which is calculated as 0.622%. This decreases the crack initiation strain to about 1.3% in 90°-plies. Cracks do not form in 45°-plies. The normalized crack density is found to rise quickly and the maximum normalized crack density at $\varepsilon_x = \varepsilon_{1T}$ is predicted to be about 0.15, much smaller than that in the Test Case 7. Some nonlinearity in stress–strain responses due to cracking is observed.

Test Case 12 and 13. Although these test cases are meant for compressive and tensile strength of the quasi-isotropic laminates in the presence of hole, we do not attempt full analysis and prediction here since that would require detailed structural stress analysis. However, we illustrate how SDM model could be applied to laminate cases where ply thickness varies. For given ply layup [45$_m$/90$_m$/−45$_m$/0$_m$]$_s$ in Test Case 13, we vary m
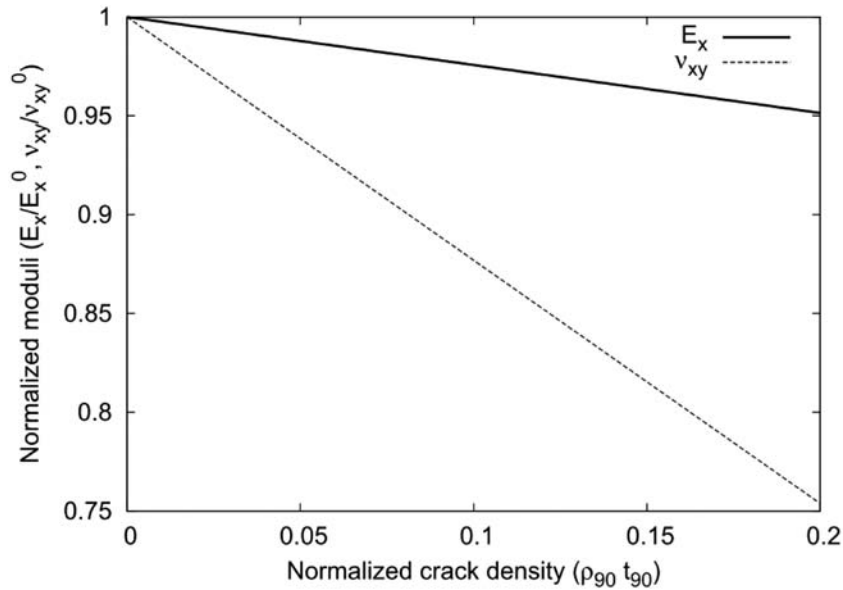
Figure 14. Stiffness and Poisson's ratio degradation for Test Case 8: $[45/0/90/-45]_s$ G4 $-$ 800/5200 laminate.
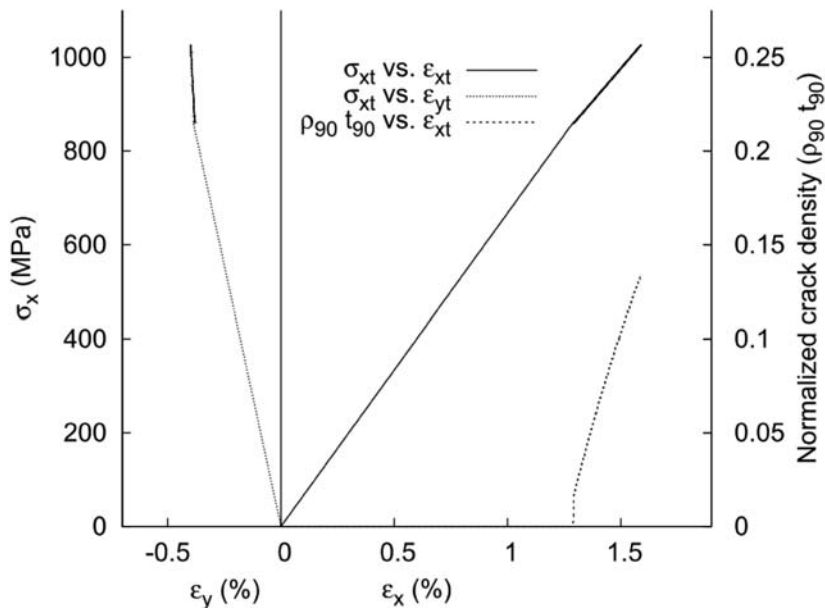
Figure 15. Stress–strain response and crack density evolution for Test Case 8: $[45/0/90/-45]_s$ G4 $-$ 800/5200 laminate with cracks in 90°-plies only. Strains generated due to thermal mismatch between 0°- and 90°-plies during curing were taken into account while evaluating damage initiation and progression.

from 1 to 4 with $m = 4$ equivalent to the Test Case 12. Cracking in only 90°-plies is assumed and the analysis neglects any damage in the ±45° and 0° plies. If there is significant cracking in 45° plies, the COD calculations (FE model) as well as stiffness predictions must account for cracks in these off-axis plies also, as was illustrated before in case of Test Case 7.

Since the ply sequence and relative thickness of cracked and constrained plies remains the same, the relative stiffness change will be given by the ratio of constraint parameters, i.e. $\beta = \kappa/\kappa_0$, where κ_0 is the constraint parameter obtained for the reference laminate $[0/90_3]_s$. β is calculated to be 0.5565, 0.5523, 0.5478 and 0.5585, respectively, for $m = 1$ to 4. Thus, the stiffness degradation should be the same in all laminates because their relative thickness is the same; the slight difference may be due to different mesh densities and inaccuracies in COD calculations. The ratio of
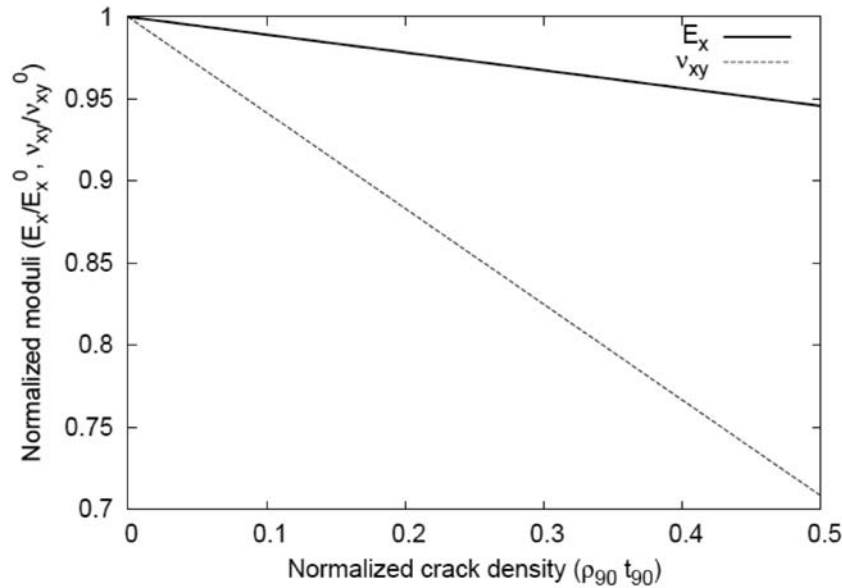
Figure 16. Stiffness and Poisson's ratio degradation for Test Case 12: $[45/90/-45/0]_s$ IM7/8552 laminate. For Test Case 13, $[45_m/90_m/-45_m/0_m]_s$ laminate, with different m values, the stiffness reduction is about the same because relative thickness of cracked and constraining plies remains constant. Cracking only in 90°-plies is assumed.
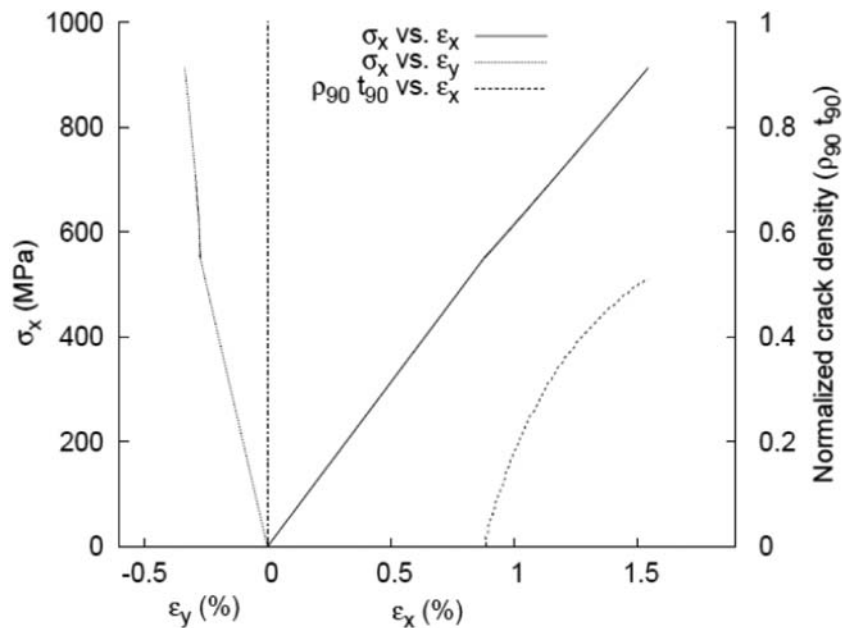
Figure 17. Stress–strain response and crack density evolution for Test Case 12: $[45/90/-45/0]_s$ IM7/8552 laminate with cracks in 90°-plies only. No thermal effects were taken into account.

degraded to original longitudinal modulus and Poisson's ratio for $m=4$ (Test Case 12) is shown in Figure 16. However, the change in thickness has a significant effect on crack initiation and progression. The crack initiation strain decreases as the cracked ply thickness increases. The rate of damage progression is higher for lower m. For a ply thickness of 0.125 mm ($m=1$), crack initiation strain was calculated to be 1.79%, which is greater than the longitudinal tensile failure strain ($\varepsilon_{1T}=1.551\%$) for the UD lamina with this material. Thus, for this value of m and the provided G_{Ic} value, our model predicts no ply cracking before
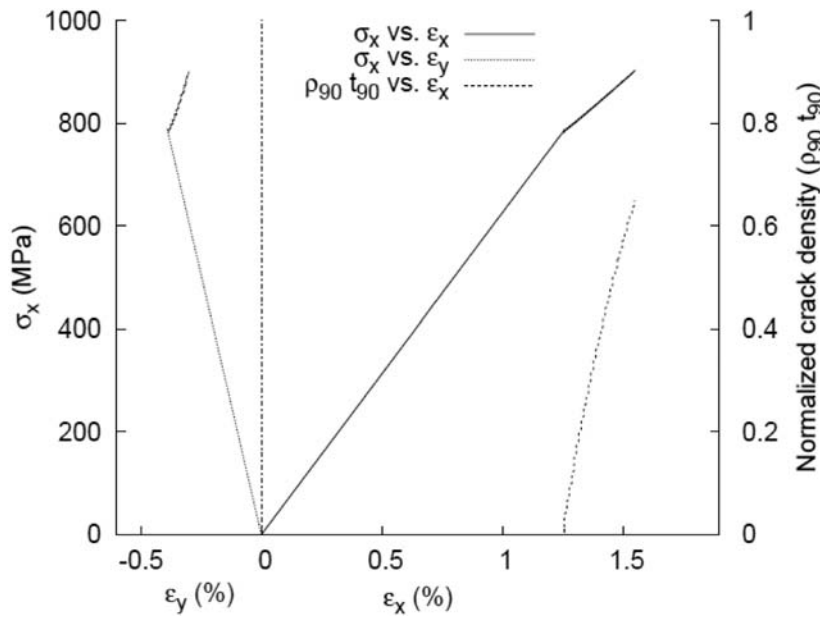
Figure 18. Stress–strain response and crack density evolution for Test Case 13: $[45_m/90_m/-45_m/0_m]_s$ IM7/8552 laminate, $m = 2$, with cracks in 90°-plies only. No thermal effects were taken into account.
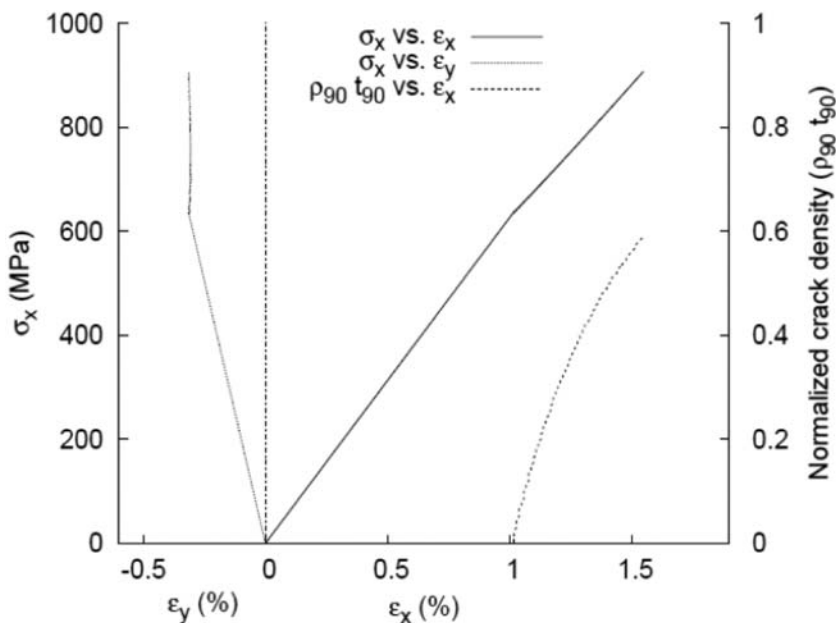
Figure 19. Stress–strain response and crack density evolution for Test Case 13: $[45_m/90_m/-45_m/0_m]_s$ IM7/8552 laminate, $m = 3$, with cracks in 90°-plies only. No thermal effects were taken into account.

laminate fails in tension by fibre fracture. For other thickness cases, the crack initiation strains for 90°-ply cracking are calculated to be 1.25%, 1.0% and 0.8%, respectively, for increasing m from 2 to 4. The normalized crack density $\rho_{90}t_{90}$ at $\varepsilon_x = \varepsilon_{1T}$ is observed to be in the neighbourhood of 0.6 for different thickness values. For thinner 90°-plies, $\rho_{90}t_{90}$ tends to reach a higher value.

For higher m values, the degradation in the Poisson's ratio is observed to be more pronounced than the degradation observed in the longitudinal Young's modulus, probably due to a very high longitudinal stiffness of the material. This was also observed earlier for G4-800/5260 material, as illustrated in Test Case 7. For Test Cases 12 and 13, this can be seen from the transverse stress–strain curves, shown

in Figure 17–19, for $m = 4$, $m = 2$ and $m = 3$, respectively. The stress–strain curves show larger nonlinearity for lower m.

It is noteworthy here that the strain at which the initiation of damage in the $90°$ plies takes place decreases with increasing the thickness of the ply (i.e. increasing the value of 'm') even when the relative thicknesses of different plies remains the same. This appears to be in a stark contrast to what strength-based failure model would predict. A strength-based model would predict the strain to be the same as long as the thickness of all the plies ($45°$, $90°$, $-45°$ and $0°$ plies) increases by the same amount. The variation of crack initiation strain with increasing m depends on change in average COD and CSD and cracked ply thickness. Since COD varies linearly with the crack size (or the cracked ply thickness), the normalized average COD is same for different m values. Therefore, the cracking criterion in equation (30) suggests $(\varepsilon)_{init} \sim 1/\sqrt{m}$. In our analysis, we have used COD values computed from FE analysis and is therefore thought to be more accurate. For large value of m, it is expected that the crack initiation strain may decrease to a small value, but the rate of decrease is asymptotic. For instance, if $m = 10$, a linear variation ($\sim 1/m$ law) suggests $(\varepsilon_x)_{init} \approx 0.25\%$ and $(\varepsilon)_{init} \sim 1/\sqrt{m}$ suggests $(\varepsilon_x)_{init} \approx 0.56\%$. Therefore, even for large m, $(\varepsilon_x)_{init}$ is not expected to reach zero value. Moreover, for high values of m, cracks in $90°$ plies actually trigger initiation of cracks in neighbouring $45°$ plies due to high crack tip stresses. In fact, experiments have shown that in a quasi-isotropic laminate of $[0/90/-45/45]_s$ sequence, cracks in $90°$ plies triggered cracks in neighbouring $45°$ ply from $0/90$ interface.

Discussion

The SDM methodology summarized above has been illustrated by taking some of the Test Cases specified in WWFE-III. The test cases and the input data have been devised for a wide range of models and are therefore not all suited to test the SDM predictions. These predictions are concerning initiation and progression of ply cracking in laminates and the consequent changes in the laminate elastic response. The inputs needed for calculating the initiation and progression of ply cracking consist of the ply elastic constants and failure properties. The conventional failure properties used in literature are normal and shear strengths as well as fracture toughness values in crack opening and shearing modes. Our approach uses none of these but instead deduces work of fracture values from crack progression data for a reference laminate. Since this was not feasible for the test cases, we used the fracture toughness data. For laminate stiffness predictions due to ply cracking,

the input data needed are ply elastic constants. The additional laminate-dependent constants needed are calculated either from test data or from FE models of representative unit cells. Of particular significance among these constants are constraint parameters that characterize surface displacements of ply cracks.

The test cases chosen have been with regard to the linear elastic response changes due to multiple ply cracks in multiple orientations. It is known that the shear stress–strain response of a ply (unidirectional composite) is nonlinear. Part of this nonlinearity can be attributed to the resin shear deformation while another part could come from shear-induced ply damage. In previous works, these aspects have been treated.[18,20] Since additional input needed for this treatment was not available, we have not applied it to the test cases here.

As a matter of general interest to damage analysis, it is noted that the elastic moduli corresponding to a given state of damage must be obtained from slopes of the unloading part of the stress–strain response. During unloading, the state of damage is constant and the strain response is reflective of the surface displacements of the ply cracks and is unaffected by any inelastic deformation that may have occurred during loading.

It is further noted that the linearized version of the stiffness-damage relationships used here makes it possible to calculate stiffness changes by adding the effects of individual damage modes (ply cracks in different orientations). Thus, as long as the state of damage is determined by a damage evolution analysis, the consequent stiffness changes can be calculated by superposition. The global loading on the laminate can be uniaxial or biaxial, it would not matter, as the resulting in-plane stress state in a cracking ply would in all cases govern the formation and multiplication of cracks. The criterion for multiple cracking used here is, however, not the critical stress state ("strength"), but the work required to open (i.e. form) ply cracks in the presence of pre-existing cracks.

Finally, it is noted that the SDM methodology is not for failure prediction in the sense of loss of load-bearing capability. It is for estimating the loss of stiffness (deformational resistance). For composite structures where reduced capacity to resist deformation is undesirable, the loss of stiffness can be equated to failure.

Conclusions

In this paper we, have briefly summarized the SDM methodology developed in previous works to evaluate effect on stiffness properties of ply cracking in multidirectional composite laminates. This multiscale methodology overcomes the limitations of the traditional

CDM formulation by application of appropriate constraint parameters that are obtained through computational micromechanics (using FEM). The required-damage related constants in the formulation for general laminates can be evaluated from data for a reference laminate, obtained from experimentation or from independent numerical calculations. The SDM formulation is thus quite suitable for design of composite laminates in the industry and can be easily coded into a commercial FE package.

Among the test cases specified in the present failure exercise, we have selected those that are suited for illustrating the SDM methodology. This methodology evaluates stiffness changes for given damage states (ply cracking densities) and for a complete description of laminate stress–strain response the evolution of damage states must be additionally determined. This is illustrated for the selected test cases by applying a recently developed damage evolution theory by the authors.[25] It is noted, however, that the laminate material constant (critical work of multiple cracking) needed in that theory requires its determination from damage evolution data. Since that was not possible here, we have instead used the fracture toughness provided in the failure exercise.

It is worth pointing out that the predictions from the present theory have been compared with those obtained from other 11 models, employed in the WWFE-III, in Reference [34]. Furthermore, a comparison between the model's predictions and experimental results will be made in Part B of the WWFE-III, planned as a special issue of *J Compos Materials*.

Conflict of interest

None declared.

References

1. Hinton MJ and Soden PD. Predicting failure in composite laminates: the background to the exercise. *Compos Sci Technol* 1998; 58(7): 1001–1010.
2. Hinton MJ, Kaddour AS and Soden PD. Evaluation of failure prediction in composite laminates: background to 'part b' of the exercise. *Compos Sci Technol* 2002; 62(12–13): 1481–1488.
3. Kaddour AS, Hinton MJ, Li S, et al. The background to part A of the Third World-Wide Failure Exercise (WWFE-III). To be published in *J Compos Mater*.
4. Zhang D, Ye J and Lam D. Ply cracking and stiffness degradation in cross-ply laminates under biaxial extension, bending and thermal loading. *Compos Struct* 2006; 75(1–4): 121–131.
5. Ye J, Lam D and Zhang D. Initiation and propagation of transverse cracking in composite laminates. *Comput Mater Sci* 2010; 47(4): 1031–1039.
6. Zhang D, Ye J and Lam D. Properties degradation induced by transverse cracks in general symmetric laminates. *Int J Solids Struct* 2007; 44(17): 5499–5517.
7. Talreja R. Transverse cracking and stiffness reduction in composite laminates. *J Compos Mater* 1985; 19(4): 355–375.
8. Talreja R. A continuum-mechanics characterization of damage in composite-materials. *Proc Roy Soc Lond Ser A* 1985; 399(1817): 195–216.
9. Talreja R. Internal variable damage mechanics of composite materials. In: Boehler JP (ed.) *Yielding, damage, and failure of anisotropic solids*. London: Mechanical Engineering Publications, 1990, pp.509–533.
10. Talreja R. Damage mechanics of composite materials based on thermodynamics with internal variables. In: Cardon A and Verchery G (eds) *Polymer based composite systems for structural applications*. London: Elsevier, 1991, pp.65–79.
11. Talreja R. Damage characterization by internal variables. In: Talreja R (ed.) *Damage mechanics of composite materials*. Elsevier: Amsterdam, 1994, pp.53–78.
12. Li S, Reid SR and Soden PD. A continuum damage model for transverse matrix cracking in laminated fibre-reinforced composites. *Philos Transact Roy Soc Lond, Ser A* 1998; 356(1746): 2379–2412.
13. Li S, Reid SR, Soden PD, et al. Modelling transverse cracking damage in thin, filament-wound tubes subjected to lateral indentation followed by internal. *Int J Mech Sci* 2005; 47(4–5): 621–646.
14. Highsmith AL and Reifsnider KL. Stiffness-reduction mechanisms in composite laminates. In: Reifsnider KL (ed.) *Damage in composite materials*. Philadelphia, PA: ASTM, 1982, pp.103–117.
15. Varna J, Joffe R and Talreja R. A synergistic damage-mechanics analysis of transverse cracking in [+/-theta/90(4)](s) laminates. *Compos Sci Technol* 2001; 61(5): 657–665.
16. Varna J, Joffe R and Talreja R. Mixed micromechanics and continuum damage mechanics approach to transverse cracking in [s,90(n)](s) laminates. *Mech Compos Mater* 2001; 37(2): 115–126.
17. Varna J, Akshantala NV and Talreja R. Crack opening displacement and the associated response of laminates with varying constraints. *Int J Damage Mech* 1999; 8: 174–193.
18. Varna J, Joffe R, Akshantala NV, et al. Damage in composite laminates with off-axis plies. *Compos Sci Technol* 1999; 59(14): 2139–2147.
19. Singh CV and Talreja R. Damage mechanics of composite laminates with transverse matrix cracks in multiple

orientations. In: *48th AIAA/ASME/ASCE/AHS/ASC Structures, Structural Dynamics, and Materials Conference*, Honolulu, Hawaii, USA, 23–26 April 2007. Reston, VA: American Institute of Aeronautics and Astronautics.

20. Singh CV and Talreja R. Analysis of multiple off-axis ply cracks in composite laminates. *Int J Solids Struct* 2008; 45(16): 4574–4589.

21. Singh CV and Talreja R. A synergistic damage mechanics approach for composite laminates with matrix cracks in multiple orientations. *Mech Mater* 2009; 41(8): 954–968.

22. Groves SE, Harris CE, Highsmith AL, et al. An experimental and analytical treatment of matrix cracking in cross-ply laminates. *Exp Mech* 1987; 27(1): 73–79.

23. Adkins J. Symmetry relations for orthotropic and transversely isotropic materials. *Arch Rational Mech Anal* 1960; 4: 193–213.

24. Spencer AJM. Theory of invariants. In: Eringen C (ed.) *Continuum physics*. New York, NY: Academic Press, 1971, pp.239–353.

25. Singh CV and Talreja R. Evolution of ply cracks in multi-directional composite laminates. *Int J Solids Struct* 2010; 47(10): 1338–1349.

26. Joffe R, Krasnikovs A and Varna J. Cod-based simulation of transverse cracking and stiffness reduction in [s/90n]s laminates. *Compos Sci Technol* 2001; 61(5): 637–656.

27. Ansys® Academic Research, Release 11.0.

28. Hill R. Elastic properties of reinforced solids: some theoretical principles. *J Mech Phys Solids* 1963; 11(5): 357–372.

29. Li S, Singh CV and Talreja R. A representative volume element based on translational symmetries for FE analysis of cracked laminates with two arrays of cracks. *Int J Solids Struct* 2009; 46(7–8): 1793–1804.

30. Singh CV. *Multiscale modeling of damage in multidirectional composite laminates*. PhD Thesis, Aerospace Engineering, Texas A&M University, College Station, TX, 2008.

31. Kaddour AS, Hinton MJ, Li S, et al. Mechanical properties and details of composite laminates for the test cases used in the third world wide failure exercise. To be published in. *J Compos Mater*.

32. Bailey JE, Curtis PT and Parvizi A. On the transverse cracking and longitudinal splitting behavior of glass and carbon-fiber reinforced epoxy cross ply laminates and the effect of Poisson and thermally generated strain. *Proc Roy Soc Lond Ser A* 1979; 366(1727): 599–623.

33. Tong J, Guild FJ, Ogin SL, et al. On matrix crack growth in quasi-isotropic laminates – I. Experimental investigation. *Compos Sci Technol* 1997; 57(11): 1527–1535.

34. Kaddour AS, Hinton MJ, Smith PA, et al. A comparison between the predictive capability of current matrix cracking, continuum damage and fracture criteria for fibre reinforced composite laminates: Part A of WWFE-III. To be published in. *J Compos Mater*.

35. Kashtalyan M and Soutis C. Stiffness and fracture analysis of laminated composites with off-axis ply matrix cracking. *Compos Pt A: Appl Sci Manuf* 2007; 38(4): 1262–1269.

Appendix A

Stiffness-damage relations for cracked laminate with two and three damage modes

Let us consider a case where two modes of damage are active. The irreducible integrity bases for ψ are then given by

$$
\begin{aligned}
&\varepsilon_{11}, \varepsilon_{22}, \varepsilon_{33}, \varepsilon_{23}^2, \varepsilon_{31}^2, \varepsilon_{12}^2, \varepsilon_{23}\varepsilon_{31}\varepsilon_{12}, \\
&D_{11}^{(1)}, D_{22}^{(1)}, D_{33}^{(1)}, \left(D_{23}^{(1)}\right)^2, \left(D_{31}^{(1)}\right)^2, \left(D_{12}^{(1)}\right)^2, D_{23}^{(1)}D_{31}^{(1)}D_{12}^{(1)}, \\
&D_{11}^{(2)}, D_{22}^{(2)}, D_{33}^{(2)}, \left(D_{23}^{(2)}\right)^2, \left(D_{31}^{(2)}\right)^2, \left(D_{12}^{(2)}\right)^2, D_{23}^{(2)}D_{31}^{(2)}D_{12}^{(2)}, \\
&\varepsilon_{23}D_{23}^{(1)}, \varepsilon_{31}D_{31}^{(1)}, \varepsilon_{12}D_{12}^{(1)}, \varepsilon_{23}D_{23}^{(2)}, \varepsilon_{31}D_{31}^{(2)}, \varepsilon_{12}D_{12}^{(2)}, \\
&\varepsilon_{31}\varepsilon_{12}D_{23}^{(1)}, \varepsilon_{12}\varepsilon_{23}D_{31}^{(1)}, \varepsilon_{23}\varepsilon_{31}D_{12}^{(1)}, \varepsilon_{31}\varepsilon_{12}D_{23}^{(2)}, \\
&\quad \varepsilon_{12}\varepsilon_{23}D_{31}^{(2)}, \varepsilon_{23}\varepsilon_{31}D_{12}^{(2)}, \\
&\varepsilon_{23}D_{31}^{(1)}D_{12}^{(1)}, \varepsilon_{31}D_{12}^{(1)}D_{23}^{(1)}, \varepsilon_{12}D_{23}^{(1)}D_{31}^{(1)}, \varepsilon_{23}D_{31}^{(2)}D_{12}^{(2)}, \\
&\quad \varepsilon_{31}D_{12}^{(2)}D_{23}^{(2)}, \varepsilon_{12}D_{23}^{(2)}D_{31}^{(2)}
\end{aligned}
$$

$$(A.1)$$

For a thin laminate loaded in its plane, the above set can be reduced by considering only the in-plane strain and damage tensor components. Thus, the remaining integrity bases in the Voigt notation are given by

$$
\begin{aligned}
&\varepsilon_1, \varepsilon_2, \varepsilon_6^2 \\
&D_1^{(1)}, D_2^{(1)}, \left(D_6^{(1)}\right)^2, D_1^{(2)}, D_2^{(2)}, \left(D_6^{(2)}\right)^2 \\
&\varepsilon_6 D_6^{(1)}, \varepsilon_6 D_6^{(2)}
\end{aligned}
$$

$$(A.2)$$

Using the above set of integrity bases, the most general polynomial form for $\rho\psi$, restricted to second-order terms in the strain components (assuming small strains) and first-order terms in damage tensor components (assuming small volume fraction of damage entities in the RVE), is given by

$$
\begin{aligned}
\rho_m\psi = P_0 &+ \left\{ c_1\varepsilon_1^2 + c_2\varepsilon_2^2 + c_3\varepsilon_6^2 + c_4\varepsilon_1\varepsilon_2 \right\} \\
&+ \varepsilon_1^2 \left\{ c_5 D_1^{(1)} + c_6 D_2^{(1)} + c_7 D_1^{(2)} + c_8 D_2^{(2)} \right\} \\
&+ \varepsilon_2^2 \left\{ c_9 D_1^{(1)} + c_{10} D_2^{(1)} + c_{11} D_1^{(2)} + c_{12} D_2^{(2)} \right\} \\
&+ \varepsilon_6^2 \left\{ c_{13} D_1^{(1)} + c_{14} D_2^{(1)} + c_{15} D_1^{(2)} + c_{16} D_2^{(2)} \right\} \\
&+ \varepsilon_1\varepsilon_2 \left\{ c_{17} D_1^{(1)} + c_{18} D_2^{(1)} + c_{19} D_1^{(2)} + c_{20} D_2^{(2)} \right\} \\
&+ \varepsilon_1\varepsilon_6 \left\{ c_{21} D_6^{(1)} + c_{22} D_6^{(2)} \right\} + \varepsilon_2\varepsilon_6 \left\{ c_{23} D_6^{(1)} + c_{24} D_6^{(2)} \right\} \\
&+ P_1\left(\varepsilon_p, D_q^{(1)}\right) + P_2\left(\varepsilon_p, D_q^{(2)}\right) + P_3\left(D_q^{(1)}\right) + P_4\left(D_q^{(2)}\right)
\end{aligned}
$$

$$(A.3)$$

where P_0 and c_i, $i = 1, 2, \ldots, 24$ are material constants, P_1 and P_2 are linear functions of strain and damage tensor components and P_3 and P_4 are linear functions only of the damage tensor components. Setting $\rho_m \psi = 0$ for unstrained and undamaged material, we have $P_0 = 0$; and assuming the unstrained material of any damaged state to be stress-free, we get $P_1 = P_2 = 0$ on using equation (12). Considering the virgin material to be orthotropic and proceeding in a similar manner as above, we obtain following relations for stiffness matrix of the damaged laminate

$$\mathbf{C_{pq}} = \mathbf{C_{pq}^0} + \mathbf{C_{pq}^{(1)}} + \mathbf{C_{pq}^{(2)}} \tag{A.4}$$

where $p, q = 1, 2, 6$; $\mathbf{C_{pq}^0}$ is the stiffness coefficient matrix of the virgin laminate given by (14), and the changes in stiffness brought about by the individual damage modes are represented by $\mathbf{C_{pq}^{(1)}}$ and $\mathbf{C_{pq}^{(2)}}$, which are given by

the plies. This material nonlinearity due to shear behaviour has to be taken into account separately while predicting shear modulus degradation. The procedure is reported in Reference [18].

The damage state subsequent to ply cracking in $+\theta$ and $-\theta$ plies can be represented by two damage mode tensors. For off-axis ply cracking, it is more convenient to rewrite the damage mode tensor defined in equation (4) in terms of normal crack spacing, $s_n^\theta = s_\theta \sin \theta$, where s_θ is the crack spacing in the axial direction (see Figure 20) for the ply of orientation θ. Accordingly, the damage mode tensors are given by

$$D_{ij}^{(\alpha)} = \frac{\kappa t_c^2}{s_n^\theta t} n_i n_j \tag{A.6}$$

With reference to Figure 20(b) where the orientations of the two damage modes are shown, the elements

$$
\mathbf{C_{pq}^{(1)}} = \begin{bmatrix} 2c_5 D_1^{(1)} + 2c_6 D_2^{(1)} & c_{17} D_1^{(1)} + c_{18} D_2^{(1)} & c_{21} D_6^{(1)} \\ & 2c_9 D_1^{(1)} + 2c_{10} D_2^{(1)} & c_{23} D_6^{(1)} \\ Symm & & 2c_{13} D_1^{(1)} + 2c_{14} D_2^{(1)} \end{bmatrix}
$$

$$
\mathbf{C_{pq}^{(2)}} = \begin{bmatrix} 2c_7 D_1^{(2)} + 2c_8 D_2^{(2)} & c_{19} D_1^{(2)} + c_{20} D_2^{(2)} & c_{22} D_6^{(2)} \\ & 2c_{11} D_1^{(2)} + 2c_{12} D_2^{(2)} & c_{24} D_6^{(2)} \\ Symm & & 2c_{15} D_1^{(2)} + 2c_{16} D_2^{(2)} \end{bmatrix} \tag{A.5}
$$

Let us now consider a special case of a general laminate undergoing damage in two symmetrically placed damage modes, such as $[0_m / \pm \theta_n / \varphi_p]_s$, with φ restricted to angles that do not cause ply cracking. In such laminates, an in-plane tensile loading will produce an in-plane stress state in each off-axis ply consisting of normal stresses along and perpendicular to fibres in that ply and a shear stress in the plane of the ply. Depending on the values of θ, φ and ply properties, the stress perpendicular to the fibres could be tensile or compressive. Thus, on loading, an off-axis ply may or may not develop intralaminar cracks. When $\theta = 90°$, the matrix will undergo multiple cracking in the transverse plies. For other cases of off-axis ply orientations, multiple cracking is typically observed to occur for angles from 50° to 90°. However, it has been observed that even in cases where these cracks do not initiate in the off-axis plies, the laminate moduli change with the applied load due to shear stress-induced damage within

of the damage mode tensor are given by

$$\text{For } \alpha = 1: \ n_i^{(1)} = (\sin \theta, \cos \theta, 0)$$

$$D_1^{(1)} = \frac{\kappa^{\theta^+} t_c^2}{s_n^{\theta^+} t} \sin^2 \theta; \ D_2^{(1)} = \frac{\kappa^{\theta^+} t_c^2}{s_n^{\theta^+} t} \cos^2 \theta;$$

$$D_6^{(1)} = \frac{\kappa^{\theta^+} t_c^2}{s_n^{\theta^+} t} \sin \theta \cos \theta$$

$$\text{For } \alpha = 2: \ n_i^{(2)} = (\sin \theta, -\cos \theta, 0)$$

$$D_1^{(2)} = \frac{\kappa^{\theta^-} t_c^2}{s_n^{\theta^-} t} \sin^2 \theta; \ D_2^{(2)} = \frac{\kappa^{\theta^-} t_c^2}{s_n^{\theta^-} t} \cos^2 \theta;$$

$$D_6^{(2)} = -\frac{\kappa^{\theta^-} t_c^2}{s_n^{\theta^-} t} \sin \theta \cos \theta \tag{A.7}$$

where the superscripts θ^+ and θ^- indicate variables for $+\theta$ and $-\theta$ plies, respectively. Assuming that the
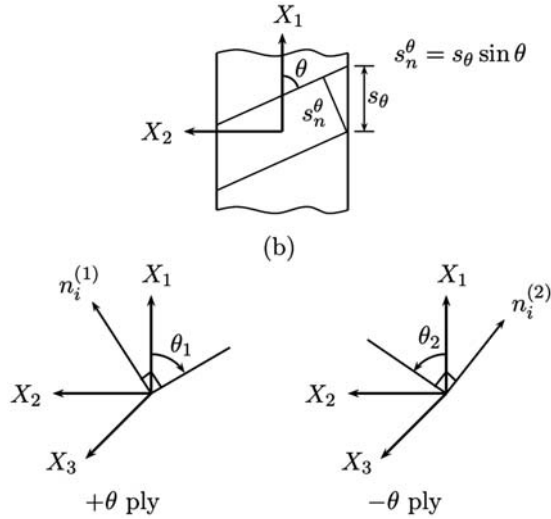
Figure 20. Damage characterization for two-damage modes. X_1, Y_1, Z_1 here refer to the global coordinate axes (same as x, y, z).

intensity and distribution of damage is same in θ^+ and θ^- plies, we have

$$\kappa^{\theta^+} = \kappa^{\theta^-} = \kappa^\theta; \quad s_n^{\theta^+} = s_n^{\theta^-} = s_n^\theta \quad (A.8)$$

Substituting (A.8) into (A.5), we obtain

$$C_{11}^{(1)} + C_{11}^{(2)} = 2\frac{\kappa_\theta t_c^2}{s_n^\theta t}\left[(c_5 + c_7)\sin^2\theta + (c_6 + c_8)\cos^2\theta\right]$$

$$C_{22}^{(1)} + C_{22}^{(2)} = 2\frac{\kappa_\theta t_c^2}{s_n^\theta t}\left[(c_9 + c_{11})\sin^2\theta + (c_{10} + c_{12})\cos^2\theta\right]$$

$$C_{66}^{(1)} + C_{66}^{(2)} = 2\frac{\kappa_\theta t_c^2}{s_n^\theta t}\left[(c_{13} + c_{15})\sin^2\theta + (c_{14} + c_{16})\cos^2\theta\right]$$

$$C_{12}^{(1)} + C_{12}^{(2)} = \frac{\kappa_\theta t_c^2}{s_n^\theta t}\left[(c_{17} + c_{19})\sin^2\theta + (c_{18} + c_{20})\cos^2\theta\right]$$

$$C_{16}^{(1)} + C_{16}^{(2)} = \frac{\kappa_\theta t_c^2}{s_n^\theta t}\sin\theta\cos\theta[-c_{21} + c_{22}] = 0$$

$$C_{26}^{(1)} + C_{26}^{(2)} = \frac{\kappa_\theta t_c^2}{s_n^\theta t}\sin\theta\cos\theta[-c_{23} + c_{24}] = 0$$

$$(A.9)$$

Thus,

$$\mathbf{C}_{pq}^{(1)} + \mathbf{C}_{pq}^{(2)} = \begin{bmatrix} 2a_1 D_1 + 2b_1 D_2 & a_4 D_1 + b_4 D_2 & 0 \\ & 2a_2 D_1 + 2b_2 D_2 & 0 \\ Symm & & 2a_3 D_1 + 2b_3 D_2 \end{bmatrix} \quad (A.10)$$

where the superscripts for denoting damage mode have been dropped for convenience, and a_i and b_i; $i = 1,2,3,4$ are the two sets of four material constants, given by

$$a_1 = c_5 + c_7, \quad a_2 = c_9 + c_{11}, \quad a_3 = c_{13} + c_{15},$$
$$a_4 = c_{17} + c_{19};$$
$$b_1 = c_6 + c_8, \quad b_2 = c_{10} + c_{12}, \quad b_3 = c_{14} + c_{16},$$
$$b_4 = c_{18} + c_{20}$$

$$(A.11)$$

Here, a_i and b_i are functions of θ. Denote,

$$a_1(\theta) = a_1\sin^2\theta + b_1\cos^2\theta,$$
$$a_2(\theta) = a_2\sin^2\theta + b_2\cos^2\theta,$$
$$a_3(\theta) = a_3\sin^2\theta + b_3\cos^2\theta,$$
$$a_4(\theta) = a_4\sin^2\theta + b_4\cos^2\theta$$

$$(A.12)$$

Then,

$$\mathbf{C}_{pq}^{(1)} + \mathbf{C}_{pq}^{(2)} = D_\theta \begin{bmatrix} 2a_1(\theta) & a_4(\theta) & 0 \\ & 2a_2(\theta) & 0 \\ Symm & & 2a_3(\theta) \end{bmatrix} \quad (A.13)$$

where

$$D_\theta = \frac{\kappa_\theta t_c^2}{s_n^\theta t} \quad (A.14)$$

Rewriting (A.12) as

$$a_i(\theta) = a_i\sin^2\theta + b_i\cos^2\theta = a_i\sin^2\theta\left(1 + \frac{b_i}{a_i}\cot^2\theta\right) \quad (A.15)$$

Consider for the moment the case when $a_i \geq b_i$. Then,

$$\frac{b_i}{a_i}\cot^2\theta \leq 1 \quad \text{for } \frac{\pi}{4} \leq \theta \leq \frac{\pi}{2} \quad (A.16)$$

Also, it can be expected that

$$\frac{b_i}{a_i}\cot^2\theta \ll 1 \quad \text{for } \frac{\pi}{3} \leq \theta \leq \frac{\pi}{2}$$
$$\textit{i.e., } a_i(\theta) \approx a_i \quad \text{for } \frac{\pi}{3} \leq \theta \leq \frac{\pi}{2} \quad (A.17)$$

For this case, we have laminate stiffness matrix as

$$
\mathbf{C_{pq}} = \begin{bmatrix} \dfrac{E_x^0}{1-\nu_{xy}^0\nu_{yx}^0} & \dfrac{\nu_{xy}^0 E_y^0}{1-\nu_{xy}^0\nu_{yx}^0} & 0 \\ & \dfrac{E_y^0}{1-\nu_{xy}^0\nu_{yx}^0} & 0 \\ Symm & & G_{xy}^0 \end{bmatrix}
$$
$$
+ D_\theta \begin{bmatrix} 2a_1 & a_4 & 0 \\ & 2a_2 & 0 \\ Symm & & 2a_3 \end{bmatrix} \quad (A.18)
$$

which is of identical form to the expression for 90° cracking in a cross-ply laminate, see equation (16). Hence, the stiffness matrix of a laminate with cracking in two symmetric damage modes is quite similar in form to that of a cracked cross-ply laminate.

We will now consider a special case of cracking in three off-axis plies, of which two are symmetrically opposite of each other, and the third one is placed along the transverse direction. Thus cracking is in $+\theta$, $-\theta$ and 90° plies. For this case, the stiffness matrix of the damaged laminate is given by

$$
\mathbf{C_{pq}} = \mathbf{C_{pq}^0} + \mathbf{C_{pq}^{(1)}} + \mathbf{C_{pq}^{(2)}} + \mathbf{C_{pq}^{(3)}} \quad (A.19)
$$

$\mathbf{C_{pq}^{(1)}} + \mathbf{C_{pq}^{(2)}}$ are already known from earlier discussion. The components of third damage mode ($\alpha = 3$) corresponding to cracking in 90° ply are

$$
D_1^{(3)} = \frac{\kappa_{90} t_{90}^2}{s^{90} t}, \ D_2^{(3)} = D_6^{(3)} = 0 \quad (A.20)
$$

The integrity bases (A.2) has additional components for $D_1^{(3)}$. The free energy function thus gets the following terms added to (A.3)

$$
\rho\psi(\alpha = 3) = a_1'\varepsilon_1^2 D_1^{(3)} + a_2'\varepsilon_2^2 D_1^{(3)} + a_3'\varepsilon_6^2 D_1^{(3)} + a_4'\varepsilon_1\varepsilon_2 D_1^{(3)} \quad (A.21)
$$

where a_i', $i = 1, 2, 3, 4$ are additional material constants. Putting (A.21) into (12), we obtain

$$
\mathbf{C_{pq}^{(3)}} = D_1^{(3)} \begin{bmatrix} 2a_1' & a_4' & 0 \\ & 2a_2' & 0 \\ Symm & & 2a_3' \end{bmatrix} \quad (A.22)
$$

where contribution to the shear components is zero.

It is important to emphasize here that the relative location of different damage modes in the whole laminate will cause different loss in stiffness due to damage in the laminate. To illustrate this let us consider two specific examples of laminates with damage modes considered in the present section, viz., $+\theta$, $-\theta$ and 90°:

laminates with $[0_m/\pm\theta_n/90_r]_s$ and $[0_m/90_r/\pm\theta_n]_s$ configurations, respectively.

Considering first the case of $[0_m/\pm\theta_n/90_r]_s$ laminate, we note that $\pm\theta$ modes occur twice in the whole laminate, above and below the mid-plane of the laminate, whereas 90° mode occurs only once. Thus, $\Delta\mathbf{C_{pq}} = \mathbf{C_{pq}} - \mathbf{C_{pq}^0} = \sum_{\alpha=1}^{N} \mathbf{C_{pq}^{(\alpha)}}$ is given by

$$
\Delta\mathbf{C_{pq}} = 2\left\{\mathbf{C_{pq}^{(1)}}(+\theta) + \mathbf{C_{pq}^{(2)}}(-\theta)\right\} + \mathbf{C_{pq}^{(3)}}(90) \quad (A.23)
$$

Collecting terms from equation (A.18) and equation (A.22) while assuming a_is to be independent of θ, we get

$$
\Delta\mathbf{C_{pq}} = 2D_\theta \begin{bmatrix} 2a_1 & a_4 & 0 \\ & 2a_2 & 0 \\ Symm & & 2a_3 \end{bmatrix}
$$
$$
+ D_{90} \begin{bmatrix} 2a_1' & a_4' & 0 \\ & 2a_2' & 0 \\ Symm & & 2a_3' \end{bmatrix} \quad (A.24)
$$

where, for the laminate configuration considered,

$$
D_\theta = \frac{\kappa_\theta (2nt_0)^2}{s_n^\theta t}; \quad D_{90} = \frac{\kappa_{90}(2rt_0)^2}{s^{90} t} \quad (A.25)
$$

where t_o denotes the thickness of a single ply. In the special case when $\theta = 90°$, $\Delta\mathbf{C_{pq}}$ as given by (A.24) should be equal to that given by a single 90° mode with crack size of $(4n + 2r)$ plies. Consider for example $\Delta\mathbf{C}_{11}$ term. If we assume that the normal crack spacing is the same in all cracked plies, then $\Delta\mathbf{C}_{11}$ for $[0_m/\pm\theta_n/90_r]_s$ laminate at $\theta = 90°$ from (A.24) is given by

$$
\Delta\mathbf{C}_{11} = 2\left\{\mathbf{C}_{11}^{(1)} + \mathbf{C}_{11}^{(2)}\right\} + \mathbf{C}_{11}^{(3)} = 4D_\theta|_{\theta=90} a_1(90) + 2D_{90}a_1'
$$
$$
= \frac{4\kappa_\theta|_{\theta=90}(2nt_0)^2}{s^{90} t} a_1 + \frac{2\kappa_{90}(2rt_0)^2}{s^{90} t}
$$
$$
a_1' = \frac{8t_0^2}{s^{90} t}\left[2n^2\kappa_\theta|_{\theta=90} a_1(90) + r^2\kappa_{90}a_1'\right] \quad (A.26)
$$

Since for $\theta = 90°$, $[0_m/\pm\theta_n/90_r]_s$ is equivalent to $[0/90_{2n+r}]_s$, we can consider their stiffness changes to be the same. Thus, $\Delta\mathbf{C}_{11}$ can also be written, using (16), as

$$
\Delta\mathbf{C}_{11} = \mathbf{C}_{11}^{(3)} = 2a_1' D_1 = \frac{\kappa_{90_{4n+2r}}[(4n+2r)t_0]^2}{s^{90} t}.2a_1' \quad (A.27)
$$

where the sub-subscript '4n + 2r' in $\kappa_{90_{4n+2,}}$ represents the crack size for 90° mode in $[0/90_{2n+r}]_s$

laminate. Equating $\Delta \mathbf{C}_{11}$ from (A.26) and (A.27), we have

$$2n^2\kappa_\theta|_{\theta=90}a_1(90) + r^2\kappa_{90}a_1' = \kappa_{90_{4n+2r}}[(2n+r)t_0]^2 a_1' \tag{A.28}$$

i.e.,

$$a_1(90) = \frac{\kappa_{90_{4n+2r}}(2n+r)^2 - r^2\kappa_{90}}{2n^2\kappa_\theta|_{\theta=90}}a_1' \tag{A.29}$$

Generalizing, we can write the interrelationship between two sets of constants as

$$a_i = \frac{\kappa_{90_{4n+2r}}(2n+r)^2 - r^2\kappa_{90}}{2n^2\kappa_\theta|_{\theta=90}}a_i' \quad i = 1,2,3,4 \tag{A.30}$$

Substituting (A.30) into (A.24), $\Delta\mathbf{C}_{pq}$ for damaged $[0_m/\pm\theta_n/90_r]_s$ laminate is given by

$$\Delta\mathbf{C}_{pq} = \bar{D}\begin{bmatrix} 2a_1' & a_4' & 0 \\ & 2a_2' & 0 \\ Symm & & 2a_3' \end{bmatrix} \tag{A.31}$$

where

$$\bar{D} = \frac{4t_0^2}{t}\left[\frac{1}{s_n^\theta}\frac{\kappa_\theta}{\kappa_\theta|_{\theta=90}}\left\{(2n+r)^2\kappa_{90_{4n+2r}} - r^2\kappa_{90}\right\} + r^2\frac{\kappa_{90}}{s^{90}}\right] \tag{A.32}$$

where the constraint parameters are given by

$$\kappa_\theta = \frac{\overline{(\Delta u_2)}_{\pm\theta_{2n}}}{2nt_0}; \quad \kappa_{90_{4n+2r}} = \frac{\overline{(\Delta u_2)}_{90_{4n+2r}}}{(4n+2r)t_0}; \quad \kappa_{90} = \frac{\overline{(\Delta u_2)}_{90_{2r}}}{2rt_0} \tag{A.33}$$

Similar analysis can be performed for $[0_m/90_r/\pm\theta_n]_s$ laminates to obtain their damage-stiffness relations, which are given in equation (21). The reader is referred to Reference [18] for details.

List of Symbols

$\overline{\Delta u_2}$	Average crack opening displacement calculated through FEM by subtracting nodal displacements in direction normal to crack surfaces
$D_{ij}^{(\alpha)}$	Components of damage mode tensor for damage mode α
κ	Constraint parameter
x, y, z	Coordinates in the global (laminate) coordinate system
x_1, x_2, x_3	Coordinates in the local (lamina) coordinate system
ρ_c	Crack density
ρ_θ	Crack density in θ-ply
G_c	Critical energy release rate
G_{Ic}	Critical energy release rate in mode I
G_{IIc}	Critical energy release rate in mode II
α	Damage mode
u, v, w	CDisplacements in global coordinate system
$E_x, E_y, G_{xy}, \nu_{xy}$	Elastic moduli for the damaged laminate
$E_x^0, E_y^0, G_{xy}^0, \nu_{xy}^0$	Elastic moduli for the undamaged laminate
$E_1, E_2, G_{12}, \nu_{12}$	Elastic moduli for the unidirectional lamina
ψ	Helmholtz free energy density
m, n, r	CIndices to denote plies in a particular orientation for the laminate layup
L	Laminate length
V	Laminate volume
W	Laminate width
ρ_m	Mass density
s_n^θ	Normal crack spacing for cracks in a ply with orientation θ
$\tilde{u}_n^\theta, \tilde{u}_t^\theta$	Normalized average crack opening and shear displacements
θ	Ply orientation
s	Spacing between two adjacent cracks
$\mathbf{C}_{pq}^{(\alpha)}$	Stiffness changes due to damage in mode α
$\mathbf{C}_{pq}^0$	Stiffness matrix for undamaged laminate
C_{ijkl}	Stiffness tensor
ε_{ij}	Strain tensor
σ_{ij}	Stress tensor
S	Surface area of a crack
t	Thickness of the whole laminate, including all plies
t_0	Thickness of a single ply
t_c	Thickness of the cracked ply
n_i	Unit normal vector for a cracked surface